Politecnico di Torino

Dipartimento Energia “Galileo Ferraris”

Master of Science in Energy and Nuclear Engineering

Tritium transport model at breeder unit level for WCLL breading blanket

Thesis advisor:
Prof. Massimo Zucchetti

Candidate:
Matteo Iacolino

Research Correlators:
Dr. Raffaella Testoni
Eng. Luigi Candido

July 23rd, 2018

Sommario

In questa tesi viene studiato il trasporto del trizio in una cella elementare appartenente al modulo equatoriale esterno del Water-Cooled Lithium-Lead (WCLL) breeding blanket del reattore a fusione DEMO.

Il trasporto del trizio è fondamentale per la valutazione di un design efficiente e per minimizzare le perdite di combustibile verso l'ambiente esterno. La modellizzazione della cella elementare permette di disporre di uno strumento che può essere adattato a qualsiasi modifica dei parametri operativi e/o della geometria. Nell'ambito della fusione nucleare, dove c'è un'elevata incertezza riguardo alle geometrie, alle proprietà termo-fisiche di trasporto e alle condizioni operative del reattore, un modello completo in grado di adattarsi ai cambiamenti progettuali continui è necessario. A tale scopo, mediante COMSOL Multiphysics®, si è sviluppato un modello 3D che tiene conto anche della termofluidodinamica del sistema, in modo da avere una stima precisa delle concentrazioni, degli inventari e delle perdite.

L'approccio multifisico ha permesso di evidenziare come i campi di temperatura, velocità e vorticità influenzino la distribuzione del trizio nei diversi domini che costituiscono la cella elementare. Il fenomeno della permeazione attraverso i materiali strutturali e attraverso l'acqua è stato descritto nel dettaglio attraverso opportune condizioni al contorno che descrivono i fenomeni alle interfacce, permettendo un'accurata valutazione delle perdite di combustibile. L'analisi in regime transitorio ha permesso di ricavare i tempi necessari affinché il sistema si assesti a valori costanti di concentrazione e, quindi, di stimare inventari e perdite.

Abstract

In this thesis the tritium transport is studied in an elementary cell belonging to the external equatorial module of the Water-Cooled Lithium-Lead (WCLL) breeding blanket of the DEMO fusion reactor.

Tritium transport is essential for the evaluation of an efficient design and to minimize fuel losses into the external environment. The modeling of the elementary cell allows to have an instrument that can be adapted to any modification of the operating parameters and/or of the geometry. In the context of nuclear fusion, where there is a high degree of uncertainty regarding the geometries, the thermo-physical and transport properties and the operating conditions of the reactor, a complete model capable of adapting to continuous design changes is mandatory. For this purpose, by means of COMSOL Multiphysics®, a 3D model that takes also into account the system thermal-fluid-dynamics has been developed in order to have a precise estimation of concentrations, inventories and losses.

The multi-physics approach allowed to highlight how the temperature, velocity and vorticity fields influence the tritium distribution in the different domains. The permeation phenomenon through the structural materials and through the water has been described in detail through appropriate boundary conditions that describe the phenomena at the interfaces, allowing an accurate assessment of the fuel losses. The analysis in a transient regime allowed to obtain the time necessary for the system to reach constant concentration values and, therefore, to evaluate inventories and losses.

Contents

List of Figures

List of Tables

List of Acronyms

ALARA	As Low As Reasonably Achievable
APS	Air plasma spray
BB	Breeding blankets
BSS	Back Support Structure
BUs	Breeder Units
CECE	Combined Electrolysis and Catalytic Exchange
CPs	Cooling plates
CVD	Chemical vapor deposition
D	Deuterium
DE	Direct Electrolysis
FCI	Flow channel insert
FPP	Fusion power plants
FW	First Wall
GTE	General transport equation
HD	Hot dipping
HT	Heat Transfer
IB/OB	Inboard outboard blanket
ISS	Isotope Separation System
LM	Laminar flow
LPCE	Liquid Phase Catalytic Exchange
LPPS	Low pressure plasma spray
MHD	Magneto Hydro Dynamics
PAV	Permeation against vacuum
PRF	Permeation reduction factor
RAMF	Reduced-activation ferritic/martensitic
SPF	Turbulent Flow
T	Tritium

TBR	Tritium breeding ratio
TDS	Transport of Diluted Species
TER	Tritium Extraction and Removal System
TES	Tritium Extraction System
TPB	Tritium Permeation Barrier
VPCE	Vapor Phase Catalytic Exchange
VPS	Vacuum plasma spray
WCLL	Water-cooled Lithium Lead
WD	Water Distillation
WDS	Water Detritiation System

1 Introduction

1.1 Aims of this work

In thermonuclear fusion reactors, the fuel is a high temperature deuterium-tritium plasma, in which tritium is bred by lithium isotopes present in solid ceramic breeder (e.g.. Li_4SiO_4, lithium-orthosilicate) or inside liquid metals (e.g., Pb-15.7Li eutectic alloy) [1]. In the breeding areas, a significant fraction of the tritium produced is extracted from the breeding zone and is used as a fuel for the D-T mixture. The tritium produced in the breeding blanket by neutrons interacting with lithium nuclei can permeate into the metal structures, and can be lost to the environment. Tritium in metallic components should therefore be kept under close control throughout the fusion reactor lifetime.

Total tritium losses from a generic fusion power plant are often considered a key parameter to evaluate the tritium containment capabilities of a nuclear plant. Without any tritium control techniques, permeation can be quite significant, thus systems like Tritium Detritiation System (TDS) and Tritium Removal System (TER) are required in order to extract tritium from both the flowing lithium lead alloy and the water in a dedicated sub-system.

The main objective of this work is to study the transport of tritium within the Water-cooled Lithium Lead (WCLL) breeding blanket of DEMO. The modelling of a single cell located in the equatorial outboard module has been performed. This model has been accomplished by developing simulations of the following components: lead-lithium channel, coolant (water) pipes, EUROFER structures (baffle, horizontal stiffening plates and pipes). The tritium inventory and the tritium losses are determined by a numerical model able to describe the different tritium concentration in the different domains. The multiphysics approach regards several physics as diffusion, permeation, laminar flow and heat transfer, that have been coupled by opportune boundary conditions.

1.2 A general overview of the European DEMO reactor

The conceptual design of the Demonstration Fusion Power Reactor (DEMO) is under development within the leadership of EUROfusion Consortium with EU H2020 funds. DEMO will be the first prototype fusion reactor designed to prove the capability to produce electrical power in a commercially acceptable way on the experience of ITER (International Thermonuclear Experimental Reactor).

ITER is a D-T reactor where plasma confinement is obtained in a magnetic field within a Tokamak. The construction is underway at Cadarache, in the south of France, by ITER consortium. The construction of the ITER Tokamak complex started in 2013 and the building costs are now over US$14 billion as of June 2015 [2]. The ITER fusion reactor has

been designed to produce 500 [MW] of output power for around twenty minutes while needing 50 [MW] to operate.

The key factors in that endeavor is the achievement of certain level of plant availability. Therefore, RAMI (Reliability, Availability, Maintainability and Inspectability) will be a key element in the engineering development of DEMO [3]. It describes a process whose primary purpose is to make sure that all the systems of the DEMO machine will be reliable during the operation phase and maintain their performance under operational conditions with the best possible availability. Failure of only one small function might result in the machine being halted for long periods of time and result in high costs for repairs and replacements. It is therefore important that every system undergoes a technical risk analysis to evaluate what can go wrong, where and when, and to recommend spare components, back-up systems, increased frequency maintenance schedules, component standardization, systems design optimization, etc. This to reduce the risk level of a main function breakdown and to decrease the time to repair both to a minimum.

A fusion power reactor system consists of burning plasma confined in a tokamak, plasma support system (magnets, plasma heating and current drive, plasma fueling), fusion nuclear core, and balance of plant (Figure 1). A tokamak is a toroidal machine designed by Russian physicists in the 1960s, through the magnetic confinement of the plasma, to create the conditions for thermonuclear fusion inside, in order to extract the produced energy. The hot plasma is contained in a magnetic field that keeps it away from the machine walls. The combination of two sets of magnetic coils, known as toroidal and poloidal field coils, creates a field in both vertical and horizontal directions, acting as a magnetic 'cage' to hold and shape the plasma. Plasma current by a transformer, with the central magnetic coil acting as the primary winding and the plasma as the secondary winding is induced. The heating provided by the plasma current (known as Ohmic heating) supplies up to a third of the 100 million degrees Celsius temperature required to make fusion occur. Additional plasma heating by neutral beam injection and radio frequency heating is provided [4].

The fusion nuclear core, also called the plasma chamber, consists of the blanket with integrated First Wall (FW), divertor, elements of plasma heating, fueling, and vacuum pumping ducts penetrating the blanket/FW, radiation shield, and vacuum vessel. The blanket is the key nuclear component of a fusion power system: power extraction at high temperature and tritium breeding to ensure tritium self-sufficiency. The DEMO reactor must:

- demonstrate production of 500 [MW] of electrical energy;
- resolve all physics and technical issues demonstrating reactor relevant technologies;
- achieve tritium self-sufficiency and tritium extraction/control;
- demonstrate the economic feasibility of electric power generation from nuclear fusion reactions;
- demonstrate nuclear safety and acceptable environmental impact with only low radioactivity waste;
- prove adequate Reliability / Maintainability / Availability / Inspectability (RAMI) with remote maintenance of fusion core components [5].

A fundamental parameter for the study of the reactor is the aspect ratio $A = R/a$ where A is the major radius and a the minor radius. Studies to understand the advantages and disadvantages due to variations in proportions have been carried out. Lower aspect ratio

designs implying a larger plasma volume and lower toroidal field have a higher Tritium Breeding Ratio (TBR), better vertical stability properties, and lower forces on in-vessel components during fast disruption events. Larger aspect ratio designs have the advantage that the gap between vessel and outer leg of the TF coil can be made smaller, to achieve the same value of toroidal field ripple. The majority of data from tokamaks is available around an aspect ratio of 3. Other general parameters are listed in Table 1.

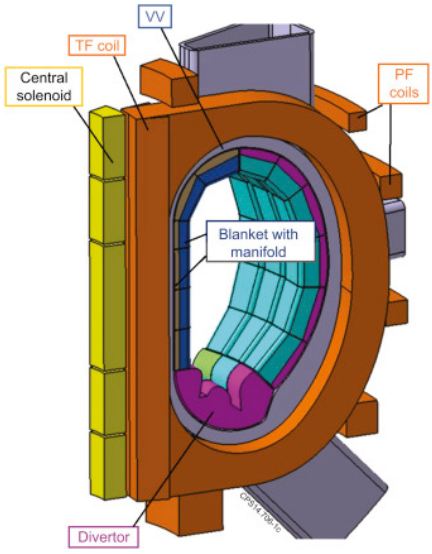

Figure 1 - Torus sector of DEMO [6].

Table 1 – DEMO key design parameters for pulsed and steady-state design options [7].

Parameter	**Symbol**	**Value**	**U.o.M.**
Major radius	R	9.1	[m]
Minor radius	a	2.9	[m]
Aspect ratio	A	3.1	
Elongation	k_{95}	1.59	
Triangularity	δ_{95}	0.33	
Plasma volume	V	2500.0	[m^3]
Tor. Magnetic field at R_0	B_0	5.7	[T]
Ma. Magnetic field at TF coil	$B_{MAX,TF}$	12.3	[T]
Safety factor	q_{95}	3.25	
Plasma current	I_p	19.6	[MA]
Greenwald density fraction	n/n_{GW}	1.2	
Confinement qualifier	H	1.1	
Auxiliary heating power	P_{ext}	50.0	[MW]
Net electric output power	P_{el}	500.0	[MW]
Plasma pulse duration	t_{pulse}	2.9	[h]

1.2.1 Different breeding Blankets

Among the proposed different concepts of Breeding Blankets (BB), the liquid breeder concepts have been extensively studied since the 1990s. The finalization of all the four breeding concepts is scheduled for 2020, in order to choose the more promising blanket to test in ITER and finally implement in DEMO [8].

The breeding blanket is one of the key systems for DEMO, as it has to ensure enough tritium production to reach the reactor tritium self-sufficiency. To ensure that there is satisfactory tritium production in a real plant the TBR in the blanket must be greater than 1 + M, where M is the breeding margin. For solid-type blanket designs, the initial TBR must be significantly higher than 1 + M, since the blanket TBR will be reduced over time as the lithium fuel is consumed. The rate of TBR reduction will affect the overall blanket self-sufficiency time, the time in which the net tritium inventory of the system is positive. The tritium breeding ratio of a fusion plant is the ratio between the amounts of generated and burnt tritium. This ratio must be defined very accurately, as the plant must not build up too much stock of the radioactive tritium, its half-life being 12.3 years. It was estimated that a breeding ratio of only a small percent above one is sufficient [9].

The tritium supply solution is to breed tritium in the blanket surrounding the region of D-T fusion reactions. The first generation for the release of energy reaction is the following:

$$D + T \rightarrow {}^{4}_{2}He(3.5\ MeV) + n(14.1\ MeV)$$

The reaction free energy is 17.6 [MeV], about 80 and 20 percent of the energy carried by neutrons and alpha particles (the helium nuclei) respectively [10].

The most favorable chemical element for breeding tritium is lithium. The nuclear reactions of primary interest are the following:

$$^{6}_{3}Li + n(slow) \rightarrow \alpha + T + 4.8MeV$$
$$^{7}_{3}Li + n(fast) \rightarrow \alpha + T + n - 2.5MeV$$

Both reactions produce tritium although the first reaction generates energy while the second one consumes energy. In addition, natural lithium comprises 7.4% Li^6 and 92.6% Li^7. Even though there is a much larger fraction of Li^7, nuclear data show that the Li^6 reaction is much easier to initiate and as a result, this reaction dominates tritium breeding. With proper selection of blanket materials, and optimized design, neutron losses by absorption or escape from the blanket can be minimized. Most neutrons slowing down to thermal energies from their initial 14.1 [MeV] energy can be absorbed by Li^6 and can generate tritium.

With respect to the Li^6 reaction, if there were no losses of neutrons, then each neutron consumed in fusion would produce one new tritium atom by breeding of a fusion-produced neutron: the breeding ratio would therefore be equal to one. In a real reactor, however, some unavoidable neutron losses always occur. Thus, some form of neutron multiplication is required. Liquid lithium appears one of the best breeding materials to use in fusion reactors from the neutronics viewpoint [11].

For acceptable tritium breeding capabilities with solid breeders, instead, neutron multipliers will be required. Beryllium is considered the best candidate. Tritium is generated inside the breeder and is diffused through lithium-lead and the blanket structures. Without proper containment, it could be released to the environment, giving a potential radiological hazard.

The blanket is located close to the vacuum vessel and it is the first structure surrounding the plasma. In addition, its coolant extracts the heat power generated by nuclear reactions, keeping blanket component temperatures under the specified design limits. EUROFER steel must be kept under 550 [°C], solid breeders under 920 [°C] [12]. Moreover, the blanket system contributes to the shielding of sensitive components behind it, e.g., the magnets. Candidate designs for the EUROfusion Breeding Blanket Project are: Water-cooled Lithium Lead (WCLL), Helium-cooled Pebble Bed (HCPB), Helium-cooled Lithium Lead (HCLL), Dual-Cooled Lithium Lead (DCLL). The last three blankets will be analyzed in the following. The WCLL, the subject of this work, will be analyzed later.

The **HCPB** BB for DEMO is based on a multi-module segment configuration, formed by 6 inboard (IB) and 6 outboard (OB) blanket modules per segment. Each blanket module is formed by a box defined by the First Wall (FW), the backplate and an arrangement of parallel Cooling Plates (CPs). At the top and bottom of each covered module, the "double" stuffing is located. Each blanket module is assembled to the Back Support Structure (BSS), as shown in Figure 2. Table 2 lists the HCPB main design parameters.

Table 2 - HCPB Blanket Concept parameters. [13]

Blanket Concept	**HCPB**	**U.o.M.**
Structural material	RAFM steel (EUROFER)	
Coolant	He	
Breeder	Solid Breeder (pebble beds) Li_4SiO_4 (Li^6 enrich. 40%) Li_2TiO_3 (Li^6 enrich. 70%)	
Temperature in/out	300/500	[°C]
Pressure	8	[MPa]
Multiplier	Be (Pebble bed) [~440]	[tons]
FW coating	2	[mm]
Helium vel. FW/SP/CP	85/40/40	[m/s]
Coolant mass flow	~2400	[kg/s]

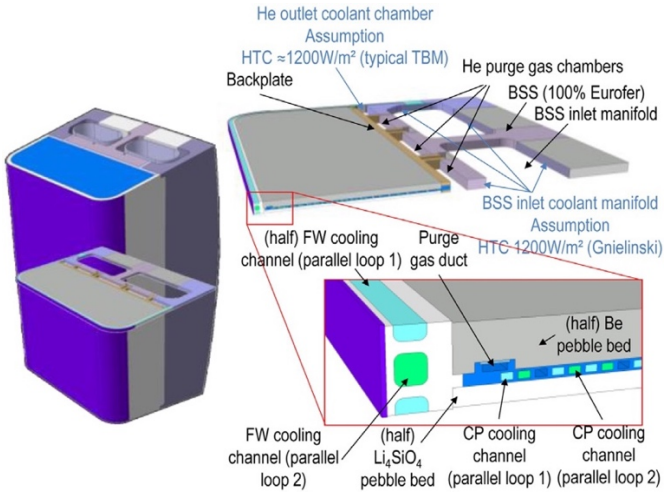

Figure 2 - Slice of HCPB [14]

HCLL blanket module consists of an EUROFER steel box formed by a U-shaped plate composing the FW and side walls, closed on its sides by side cover plates and on the back by a set of back plates and tie rods (for BSS attachments). An exploded view of the module is given in Figure 3. It is composed of a FW, externally coated with a 2 [mm] tungsten layer and two Side Walls (SWs), actively cooled by means of rectangular cooling channels. Horizontal Stiffening Plates (hSPs) and vertical Stiffening Plates (vSPs) will ensure the component to withstand the mechanical the module is subject to, and the removal of a certain percentage of the heat power deposited into the Breeder Zone (BZ) too. The SPs grid forms a Breeder Units (BUs) array, where a further set of plates, named cooling plates, cools down the liquid breeder flowing through them. All the plates, except the back plates constituting the manifolds, have internal cooling channels with a rectangular section.

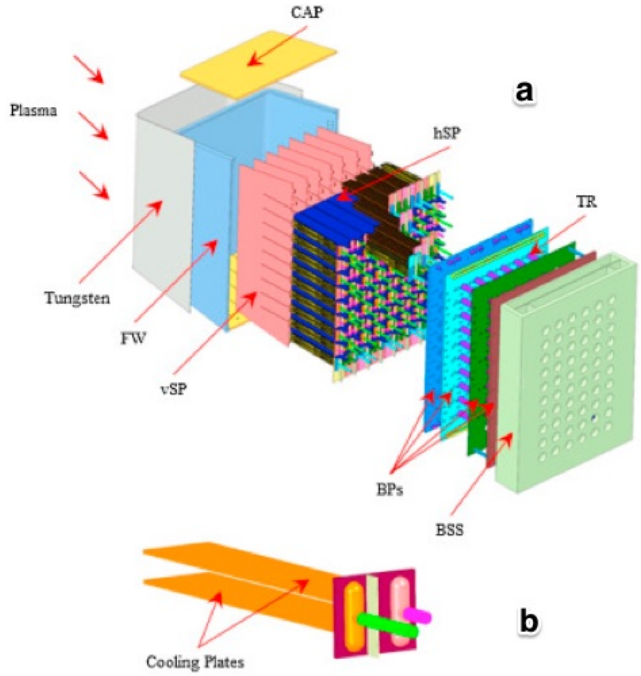

Figure 3 - a) HCLL Blanket Module; b) Detail of cooling plates configuration in the breeder unit. [15]

The **DCLL** (Figure 4) is a breeding blanket concept that potentially leads to a high-temperature (T~700 [°C]), high thermal efficiency (>40%) blanket system. In this concept, a high-temperature lithium-lead (PbLi) alloy slowly circulates (u~10 [cm/s]) in large poloidal rectangular ducts (D~20 [cm]), to remove the volumetric heat generated by neutrons and produce tritium, while a pressurized (typically to 8 [MPa]) helium gas is used to remove surface heat flux and to cool the ferritic FW and other blanket structures in the self-cooled region. The key element of this concept is a Flow Channel Insert (FCI), which serves as an electrical or electrical/thermal insulator to reduce the Magneto Hydro Dynamics (MHD) pressure drop and to decouple the temperature limited RAFM (reduced-activation ferritic/martensitic) steel wall from the flowing hot PbLi.

The reference design uses ‘banana-shape’ segments to facilitate a faster remote maintenance, in order to guarantee higher availability of the reactor. Each single module has a total channel length of 21 [m]. The module consists of 150 plates with inner He channels. Each banana module has four PbLi channels, 2 for the inlet and 2 for the outlet of the liquid metal. The PbLi inlet and outlet are on top, and PbLi enters to the first wall. The PbLi channels have

round corners for a better flow, and the flow velocity is 0.15 [m/s]. The shield is acting also as distributor and collector of the helium channels, having the dual task of He entry and exit. The shield specific part is 15 [cm] thick, and the collector function occupies other 15 [cm] [16].

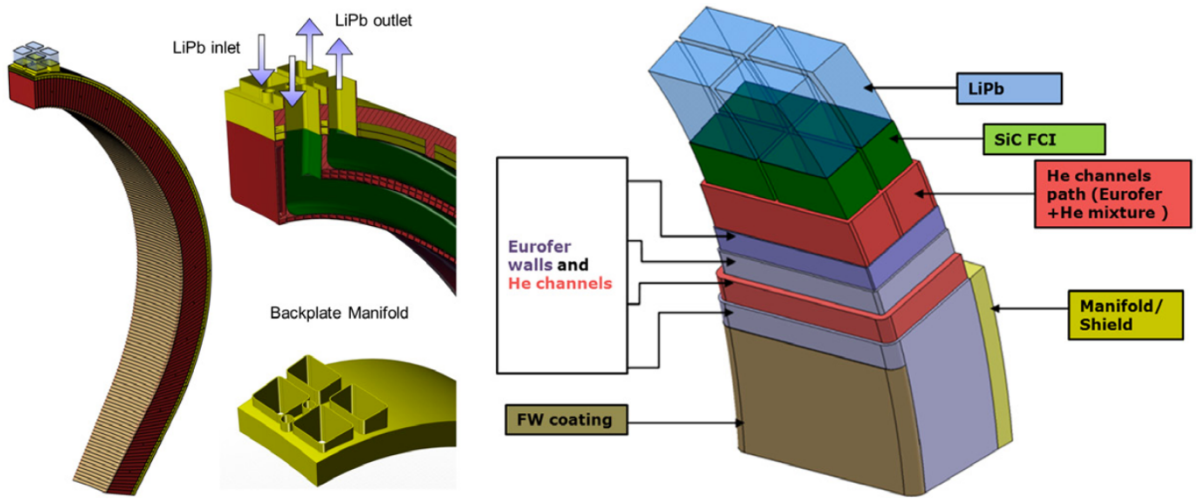

Figure 4 - 'Banana-shaped' breeding blanket module.

Blanket configurations for the different DEMO breeder blankets concepts are given in Table 3 [17]. In this view, the lithium-lead in eutectic composition (Pb-15.7Li) is a very attractive material for blanket, since it can lead to tritium self-sufficiency, it is not prone to irradiation damage and, in comparison with ceramic breeders, it has high thermal conductivity. Furthermore, it has high-energy multiplication, high tritium breeding and low tritium inventory. The low value of the tritium solubility constant is a weak point of Pb-15.7Li, resulting in a high tritium permeation rate from the liquid metal to the primary cooling system. The accurate evaluation of tritium solubility in PbLi is necessary, because this parameter directly impacts all functional properties of the blanket: in particular, the determination of tritium inventory, tritium permeation rate, and tritium extraction efficiency.

Table 3 - Basic configurations of different BB [17].

Parameter	**HCPB**	**HCLL**	**WCLL**	**DCLL**
^{6}Li enrichment, %	60	90	90	90
# of modules	20	20	15	15
BZ Material composition, %				
EUROFER steel	10	10	10	10
Breeder	15.4	80.8	87	80
Be	69	-	-	-
Water	-	-	3	-
SiC	-	-	-	7
Manifold Material composition, %				
EUROFER steel	43.4	35	43	51.3
Breeder	-	7	46	44.4
Water	-	-	11	-
Initial TBR	**1.20**	**1.14**	**1.10**	**1.14**

1.2.2 The Water Coolant Lithium-Lead breeding blanket

The WCLL breeding blanket uses high-pressure water at 155 [bar] as a coolant and liquid lithium-lead as neutron multiplier, tritium breeder and tritium carrier. The assessments presented here are based on WCLL 2015 design [1]. The new WCLL breeding blanket design has been proposed by ENEA and is conceived as a modular concept: the blanket structure is segmented in small modules with straight surfaces, attached to common BSS housing feeding pipes, in order to form a blanket segment, which can be removed from the upper port. The old CEA design, abandoned for about ten years, is featured by a monobloc architecture named "banana-shaped". In this design the breeder and the related cooling tubes are contained in cylindrical units arranged poloidally around the plasma inside the segment boxes. The number of modules and their location result from an optimization which objective is to minimize the neutron leakage in the radial direction while achieving a good temperature distribution inside the blanket. On the outboard side these cylindrical modules have a banana shape whereas on the inboard they are straight, disposed along radial rows and extending also into the space available behind the divertor plates [18].

The DEMO WCLL blanket system is divided in 18 sectors along the toroidal direction. A blanket sector has three segments in the Outboard Blanket (OB) and two segments in the Inboard Blanket (IB) with 20 [mm] gaps in between. Thus, there are 54 segments in the outboard blanket and 36 on the inboard blanket, along the toroidal direction. In poloidal direction, the blanket is divided in 7 modules in the inboard and 7 in the outboard. The blanket system has 378 modules in the outboard and 252 modules in the inboard [19].

The inboard modules have constant radial thickness of 550 [mm]. The outboard modules have radial thickness between 800 and 900 [mm]. Each module box has a quasi-modular geometry. An “elementary cell” is repeated along the poloidal direction up to the lower and upper caps, which represent a discontinuity. To ease the access and to speed up maintenance and reparation, the replacement of small modules by in-vessel remote-handling is often preferable to the replacement of larger sectors that require the cutting of the vacuum vessel and sometimes even the particularly time-consuming heating and cooling of the toroidal field coils. It is therefore expected that the segmentation of the blanket in smaller modules (e.g. three modules each for the inboard and outboard blankets plus the top board blanket), in a similar way as proposed for the TAURO self-cooled blanket, may facilitate fabrication of the structure and ease remote handling, as in the old CEA design [20].

The Equatorial Outer Central Module (EOCM) is the reference one for the geometrical description and the analyses performed. The module consists of an EUROFER steel box, reinforced by an internal grid of radial-poloidal and poloidal-toroidal plates in order to withstand water pressure (15.5 [MPa]) in case of accidental pressurization. In the breeder unit, there are 15 stiffening plates of 12 [mm] in radial-toroidal direction, and 5 stiffening plates, 16 [mm] thick (Figure 5). The module box is divided in 16 elementary cells in poloidal direction and 6 channels in toroidal direction. Each elementary cell is divided in the middle by a baffle plate: the PbLi enters in the bottom of the cell, flows in radial-poloidal direction and exits from the top of the elementary cell, as shown in Figure 5b.

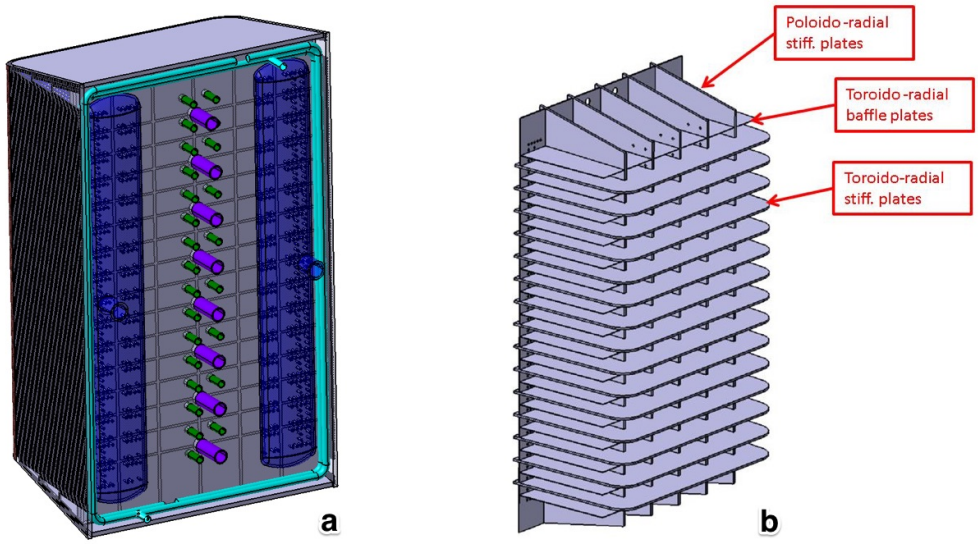

Figure 5 - a) WCLL OB4 back; b) Plates of OB 4 module [18].

The front part of the WCLL BB System is the FW. The FW is a U-shape plate bended in radial direction. with a bended radius of about 150 [mm]. The FW thickness is 25 [mm]. Moreover, the FW is covered by a tungsten layer of 2 [mm] on the plasma facing area (Figure 6a). The FW is cooled with water at 15.5 [MPa], with inlet temperature and outlet temperature of 285 [°C] and 325 [°C], respectively. The water flows in cross flow in square channels with dimension of 7x7 [mm^2] and pitch of 13.5 [mm]. The channels are inside the steel structure, along the radial-toroidal direction (Figure 6b). The top and bottom walls have the same structure of the FW, except for the layout of the cooling water channels and their pitch. In particular, 13 channels are placed on the walls in toroidal-radial direction: the channels have the same section of the first wall and are centered. The pitch is variable: the first eight channels, placed near the facing plasma, have a pitch of 16 [mm], while the others have a variable pitch from 64 to 128 [mm]. All other dimensions are reported in Table 4. The back plate is on the box back: attachments to the structure and manifolds to collect the water and the Pb-15.7Li are fixed as shown in Figure 5a.

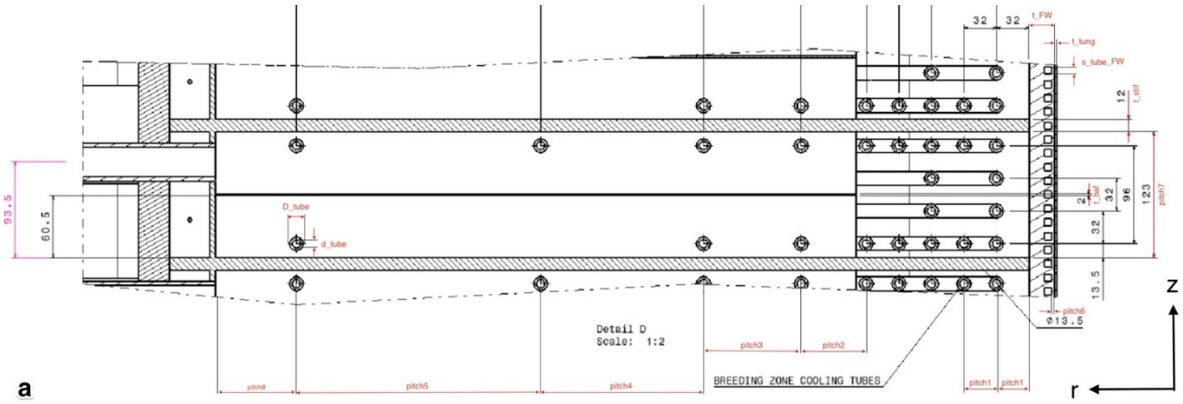

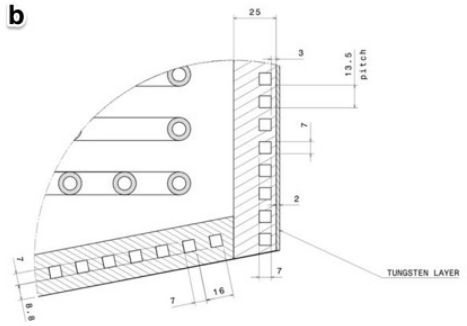

Figure 6 - a) Section of a single cell; b) FW section on poloidal plane [1].

Table 4 - Geometric Parameters WCLL.

Parameter	Value [mm]	Description
D_{out}	15.5	Water pipe external diameter
D_{in}	8	Water pipe internal diameter
t_{hSP}	12	Thickness of horizontal stiffening plate
t_{baf}	2	Thickness of the baffle
$s_{tube,FW}$	7	Length of the square water pipe
t_W	2	Tungsten thickness
t_{FW}	25	Radial length of the first wall
p_1	32	Pitch 1
$p_{2\ldots5}$	$[2, 3, 5, 7.5] \cdot p_1$	Pitch 2, 3, 4, 5
p_6	3	Pitch 6
p_7	123	Pitch 7
p_8	77	Pitch 8

1.3 DEMO relevance

In the European development pathway to fusion power DEMO is the only step between ITER and a commercial fusion power plant. Its general goals are:

1. Produce net electricity for the grid at the level of a few hundred MWs;
2. Produce the amount of tritium needed to close its fuel cycle;
3. Test all the technologies for the construction of a commercial Fusion Power Plants (FPP).

To meet the goal of fusion electricity demonstration by 2050, DEMO construction has to begin in the early 2030s at the latest, to allow the start of operation in the early 2050s. To meet its general goals, DEMO will have to rely on and robust technical solutions and well established regimes of operation, as far as possible extrapolated from ITER, and on the use of materials adequate for the expected level of neutron fluence. In addition, DEMO must be capable of addressing goal 3 also through the test of the advanced components and technical solutions that will be developed in parallel for application in a FPP, thus playing the role of a component test facility as part of its mission. The technologies desirable for advanced fusion power plants and as risk reduction elements, but not mature enough to be incorporated in DEMO, will have to be pursued in parallel. While ITER is under construction and DEMO in its conceptual phase, other installations with diverse characteristics and objectives are

planned, to conduct complementary research and development in the areas of advanced material development, tritium self-sufficiency, and heat exhaustion [21]. This approach, together with the R&D for risk mitigation proposed here, will foster innovation taking full benefit of the ITER experience and ensuring a single step to a commercial fusion power plant. The roadmap is articulated in eight missions. For each mission, a specific analysis of critical aspects for reactor application, technology readiness level, risks and risk mitigation strategies has been made [22].

2 The tritium cycle in DEMO

2.1 Introduction

Tritium resources are not adequate to guarantee the operation of future fusion plants; therefore, tritium self-sufficiency is a mandatory requirement for this type of machine. For any energy system, fuel resources are an important point. Since natural water or Standard Mean Ocean Water (SMOW) contains 0.016 % deuterium (D), D can be extracted from the water, mainly by means of electrolysis. Tritium is also present in nature in very small quantities; the total abundance of T on the earth is around of several kg ($\sim 3 \cdot 10^{18}$ $[Bq]$), existing with chemical form of HTO [23]. Currently, about 100 [g] of T is produced per year in a standard CANDU reactor and 20 - 25 [kg] T (mainly in Canada) will be available for operation of ITER [24]. Tritium production rate in DEMO will need to be ~100 times higher than in ITER. Therefore, a TBR greater than one is necessary, as well as a n adequate knowledge of tritium cycle, from the production in the breeder unit to the transport to other components [25]. It is thus important to assess the issues affecting tritium breeding performance. Within the Fusion Technology program, systematic analyses on the effect of various modifications to the breeding blanket configuration on the TBR were conducted.

Tritium produced in the breeding blanket by neutrons interacting with lithium nuclei can enter the metal structures, and then be lost by permeation to the environment. Therefore, tritium permeation and inventory in metallic components should be kept under close control throughout the fusion reactor lifetime, bearing in mind the risk of accidents and the need for maintenance. Without any tritium control techniques (like Tritium Extraction and Removal System (TER) and Permeation Reduction Barriers (PRF)), permeation can be quite significant: some tritium transport mitigation devices are therefore required. Minimization of tritium releases, in accordance to the ALARA (As Low As Reasonably Achievable) principle, is one of the key safety issues for fusion reactors [26]. In fact, for both safety and economic reasons, as much tritium as possible must be recovered inside the plant, for reuse within the tritium fuel cycle.

2.2 Tritium extraction technologies

Several different technologies to extract tritium and minimize losses are currently available. Figure 7a depicts the process flow diagram used for modelling of a complete lithium-lead loop. The geometry of the WCLL outboard equatorial module is rather complex, but it actually consists of two zones: the FW and the BZ. The lithium-lead enters firstly in the BZ, which is connected in series with the FW. When leaving the FW channel, the flow is multiplied by the number of breeder modules that are fed by one lithium-lead loop (an average of 76 modules per TES loop). The thermal hydrogen molecules adsorbed by the metal surface dissociate into constituent atoms. These atoms can diffuse through the bulk of the solid, or back towards the front surface. When hydrogen atoms reach the front

surface (recycling) or the back surface (permeation), before leaving the solid, they can recombine into molecules (recombination). Immediately after, the PbLi flow goes through the tritium extraction and removal system, where part of the tritium is extracted, while the rest re-enters the blanket, closing the loop. When going through the BZ and FW channel, tritium can permeate through the EUROFER (or AISI 304) walls reaching the water. Unlike the lithium-lead channels, the water pipes of the BZ and the FW run in crossflow.

The conceptual design of the TER for the European DEMO reactor is worked out in parallel for 4 different BB options: one solid and three liquid BB concepts [27]. The scopes of TER are [28]:

- Extract tritium from the flowing lithium lead alloy in a dedicated sub-system;
- Route it to the Tritium Plant for final processing.

The TER is placed at the outlet of BB in order to immediately reduce tritium concentration in the loop and therefore tritium losses.

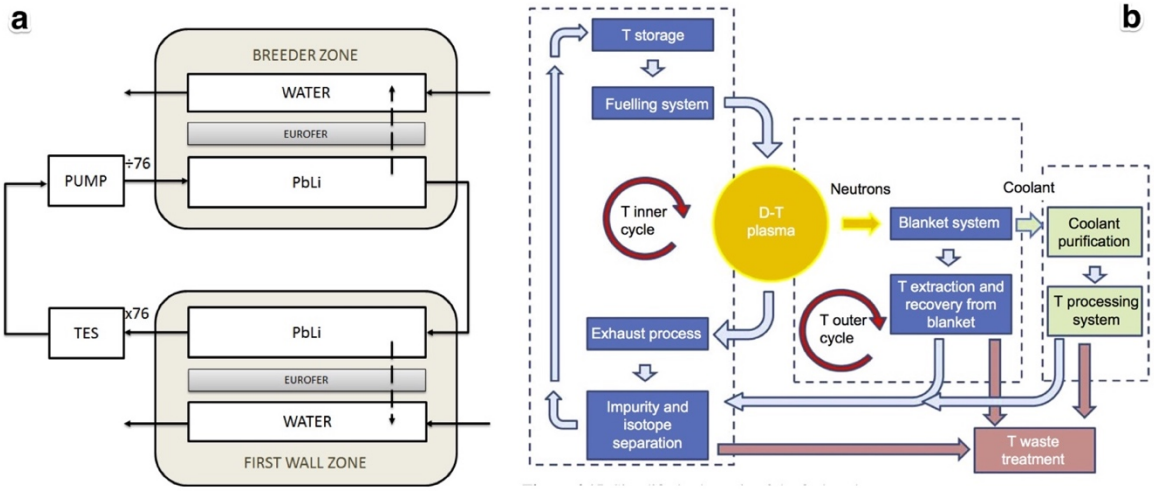

Figure 7 - a) Lithium-lead loop; b) Fuel cycle (inner-outer) [29].

Usually the injection rate has to be much larger than the actual tritium burning rate, due to produced He that stops the D-T reaction.

A first stored tritium amount constitutes the starting inventory for the plant (tritium storage). It should provide sufficient tritium for the first days as soon as the cycle arrives in a stationary condition. Tritium and deuterium are injected in the plasma. As mentioned already, only a part will burn, but the rest will leave the plasma. It will be extracted by the pumping systems, reprocessed and again sent to the storage, to feed the injection system once more. This constitutes the so-called 'inner fuel cycle'. The 'outer fuel cycle' starts with the tritium production in the blanket through breeding; this tritium is collected and processed to remove it from the different carriers (e.g. purge flow, liquid breeder, coolant), see Figure 7b. Finally, it is delivered to the separation system to be integrated in the inner cycle. Impurities are removed from the processing units and sent to the waste management system [30].

2.2.1 Tritium extraction from lithium-lead

Tritium extraction is a fundamental parameter for fuel self-sufficiency in fusion reactors. For this purpose, four different technologies have been studied: Permeators Against Vacuum (PAVs), Gas Liquid Contactors (GLCs), Regenerable getters, Droplets technologies.

The **PAVs** (Permeators Against Vacuum) technologies are at the moment the most efficient in extracting tritium from the eutectic lithium-lead alloy: they are based on the phenomenon of tritium permeation through a membrane. TRITON (TRITium permeatiON) is the name of the PAV under construction at CIEMAT. A supporting structure of stainless steel, with splines to allocate the 1 mm thick and 1 m long membrane, was designed. Fourteen sheets are needed to form 7 PbLi flowing ducts and 8 vacuum channels (Figure 8a). The structure has some lateral holes for vacuum extraction. A box containing the flange and feedthroughs for the vacuum pump, thermocouples, pressure sensors and heating elements has been designed, to complete the structure and integrate the vacuum system. The connection to the PbLi circuit is made through a round to square diffuser, to distribute the flow over the PbLi ducts (Figure 8b) [31].

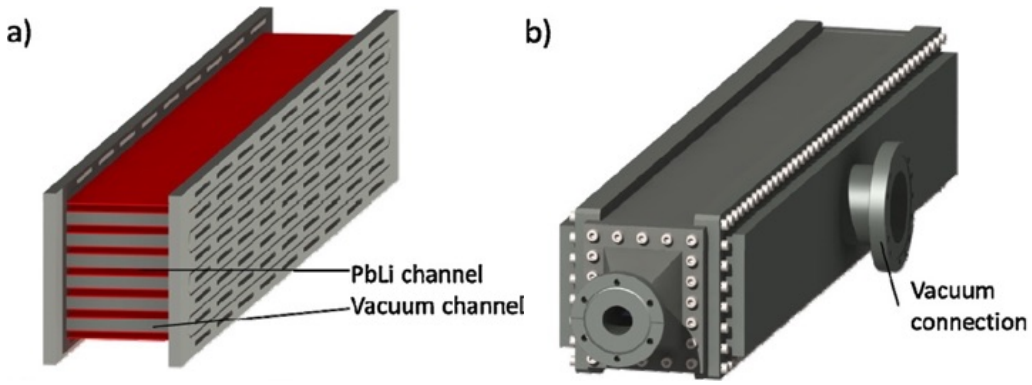

Figure 8 - Conceptual design of TRITON PAV [31].

The **GLC** packed columns are vertical columns filled with packing or any other device providing a large interfacial surface between liquid and gas phase in both countercurrent and concurrent flow (Figure 9). A gas and a liquid phase are brought into contact to obtain diffusion interchange between them. There are two groups of packing: the random packing like rings, the regular or structured packing like layered sheets. The extractor column, used for stripping of the hydrogen contained in the eutectic alloy, is of the filled type, in counter flow. The liquid phase, represented by the PbLi alloy, enters in the column from the top, passing through the filler, in hydrogen saturated conditions. A hydrogen sensor in liquid metal reads the real hydrogen content. The gaseous phase, represented by pure argon, is injected in the column from the bottom through an appropriate system of distribution that has the function to uniform and fragment the gas bubbles [32]. An experimental campaign was performed in TRIEX (TRItium Extraction) facility in ENEA Brasimone Research Centre. In TRIEX, the extraction efficiency of different technologies will be tested in a systematic way [33].

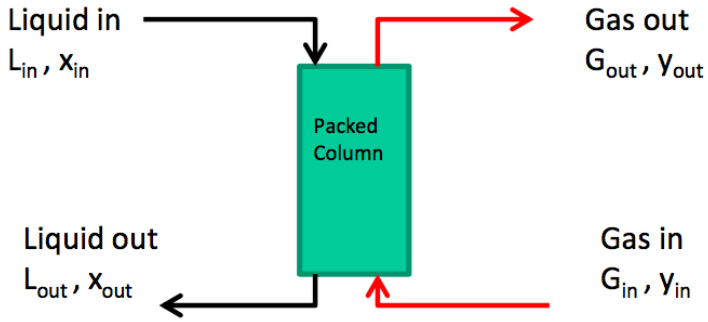

Figure 9 - GLC packed columns [35].

Non-evaporable **getters** are extensively used in vacuum technology. They find application in both industrial and laboratory fields and, generally, whenever it is necessary to remove gaseous impurities in sealed vacuum or controlled atmosphere devices. The more traditional applications include gettering in various commercial vacuum tubes. Such getters are now also being used in advanced applications such as plasma physics, controlled nuclear fusion, storage systems for tritium handling particle accelerators, where high pumping speeds and sorption capacities are of the utmost importance for hydrogen and its isotopes. High efficiency getter pumps have proved suitable to comply with these requirements. In order to regain the most favorable operating conditions, after a period of pumping, the getter device must be submitted to a regeneration process. During this treatment, carried out at a temperature higher than that of normal operation, hydrogen isotopes are desorbed and exhausted through the primary pumping system. Other irreversibly adsorbed active gases, such as CO, CO_2, N_2, O_2, are diffused into the getter bulk. Because of this treatment the original gettering properties of the material are largely restored. A knowledge of the behavior of the equilibrium pressure for the hydrogen isotopes dissolved in the getter material, as a function of the temperature and concentration, is therefore very helpful to optimize the regeneration process.

Droplets and Gas-liquid counter-current extraction tower or vacuum sieve tray. A recent study at Kyoto University [34] indicated interesting theoretical results on the vacuum sieve trays. By making small droplets in the vacuum, tritium released from droplets is collected by a vacuum pumping system (Figure 10). This method is based on the passive extraction of T from millimeter scale PbLi droplets falling in a vacuum tank. It was wrongly rejected before because the T transport within the droplet was thought to be diffusion- governed and therefore too slow [35]. Recent VST experiments showed that the droplets oscillate after detaching from the injected PbLi jet. These oscillations result in internal fluid element circulation and promote the transport of T, which is then no longer diffusion governed, towards the surface. This phenomenon can explain the significant boost measured in extraction rate and makes the VST method very promising.

To process the large PbLi mass flow rates occurring in actual breeding blankets, multiple nozzles will have to be implemented. This is because a significant increase in nozzle diameter to increase the mass flow rate would plunge the extraction efficiency. The pitch is chosen to be 1 cm which is assumed to be a conservative value to avoid coalescence and to limit the effects of reabsorption of extracted T by neighboring droplets [36].

By increasing the height of the vacuum tank up to a realistic value of 10 m, high efficiencies can be reached even for nozzles with a diameter of 1 mm. This makes the VST method a viable and promising tritium extraction system candidate. The achieved efficiency of 0.992 for this configuration is far above the minimal required efficiency of 0.8 in DEMO. Therefore, although already feasible in size, the extraction system can be made even more compact whilst keeping the efficiency higher than 0.8 by increasing the mass flow rate per nozzle. This can be achieved in 2 ways: by increasing the diameter of the nozzles or by increasing the hydrostatic pressure at the nozzle's outlet [37].

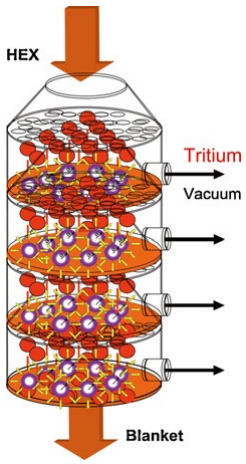

Figure 10 - Extraction tower [38].

In Table 5, the different technologies have been schematized with the respective extraction efficiencies. An analysis of current research indicates the best technology for DEMO to be the PAV in terms of efficiency and simple construction.

Table 5 - Advantages and disadvantages of TER technologies.

Technologies	Advantages	Disadvantages	Efficiency
PAV	PAV is a first choice process candidate due to its simplicity and reliability.	At high temperature it has a strong tendency to oxidation, requiring a very high vacuum during operation and/or a surface layer of Pd which is more oxidation resistant	69-90%
GLC	Reliable injection system, because it is not necessary to inject small size bubbles. Reliability of the functional answer because of the kinetics of mass transfer. The packing material could be manufactured with high corrosion resistance materials to Pb-15.7Li. The Packed columns, used as tritium extraction from lithium-lead, have been tested extensively in the past in MELODIE loop at CEA and in TRIEX at ENEA.	Lower rate size/η (tritium extraction efficiency for one column is 25-30 %) than permeators. In any case the size of the columns is a consequence of its efficiency, and the design of the columns can be optimised.	30%
Droplets	Good operation in terms of maintainability and reliability	Calculation of the absorbed tritium. Experimental characterization is on-going	45-90%

2.2.2 Tritium extraction from water

A conventional method for the confinement and removal of tritium in atmosphere is to oxidize tritium to tritiated water by a catalytic oxidizer and to remove tritiated water by molecular sieve dryers. The tritium concentration in the waste water - regenerated from these atmosphere detritiation systems - is expected to be much higher than the permitted value to discharge it to the environment. A Water Detritiation System (WDS) is thus needed. The technologies under consideration for this purpose are: Combined Electrolysis and Catalytic Exchange (CECE), Liquid Phase Catalytic Exchange (LPCE), Vapor Phase Catalytic Exchange (VPCE), Water Distillation (WD) and Direct Electrolysis (DE).

The WDS designed for ITER is based on the combined electrolysis and catalytic exchange process, to ensure that the emission of tritium into the environment is maintained below very strict limits.

The **CECE** process has a water electrolysis cell producing hydrogen and oxygen at a rate determined by the cell size [39]. In the WDS, the oxygen is sent to the air detritiation system where the tritiated hydrogen impurity is oxidized to water and all the tritiated water vapor is returned to the WDS. The hydrogen gas from the cell has a portion of its tritium removed in a side-stream that goes through the Isotope Separation System (ISS) and then is humidified and sent upwards through the isotope exchange columns (**LPCE**) (Figure 11). Water flows downward though the exchange columns, becoming enriched in tritium (and deuterium)

before entering the electrolysis cell. The total water fed to the system matches the requirements of the electrolysis cell and is made up of natural stripping water fed at the top of the LPCE column and tritiated feedwater supplied either directly to the cell or part way up the LPCE column [40].

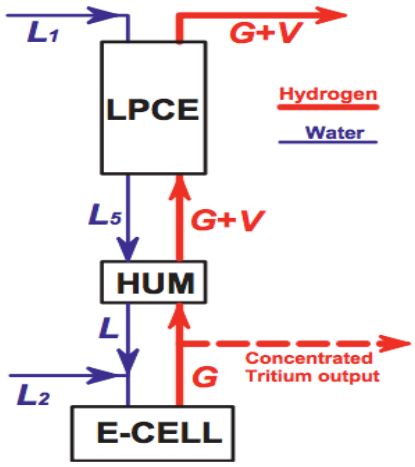

Figure 11 - Block diagram of the WDS. HUM=humidifier [41].

VPCE was developed by the French Atomic Energy Commission (CEA). Tritium and hydrogen containing deuterium oxide are first heated to a vapor. Under a certain pressure, deuterium oxide vapor mixes with D_2 at 200 [°C] and then enters the exchange column filled with a noble metal catalyst. HDO and DTO exchange with very pure D_2, the reactions are expressed by reactions:

$$HDO_{(vapor)} + D_{2(gas)} \Leftrightarrow HD_{(gas)} + D_2O_{(vapor)}$$

$$DTO_{(vapor)} + D_{2(gas)} \Leftrightarrow DT_{(gas)} + D_2O_{(vapor)}$$

In these two vapor phase catalytic exchange reactions, the ratio (L/G) of the liquid phase flow rate (L) and vapor phase flow rate (G) must be lower than the equilibrium constant of exchange reaction to achieve mass transfer of hydrogen and tritium from liquid phase to vapor phase. VPCE reactions use hydrophilic catalysts and are conducted at 200 [°C] to avoid activity reduction of hydrophilic catalysts affected by the condensation of water vapor. Tritium containing deuterium oxide needs repeated vaporization and condensation at 200 [°C]. The equipment and process are very complicated and consume much energy [42].

WD is well proven and has been used extensively for heavy water upgrading for about 45 years, up to a concentration of about 40 [Ci/kg]. Separation factors, the relationship between the enriched and depleted streams, show that WD should be about equally effective in separating tritium, if the concentrations are low. In a heavy water system, however, the separation of tritium is very poor.
Water distillation offers the safety advantage of moderate temperatures and sub-atmospheric operating pressures typically operating at 13 [kPa] (51 [°C]) at the top and 20 [kPa] (60 [°C]) at the bottom. Thus, any trace leaks in the system will be inwards, tending to minimize tritium release. Depending on the specific design, water can be enriched to significant

concentrations at the bottom of the towers, e.g., the latest estimate for the ITER Water Detritiation System is about 300 [Ci/kg]. In this case, secondary containment of the bottom portion of the WD column would be suggested, since WD columns are not commonly used with these relatively high concentrations. The purpose of the secondary containment would be to mitigate the consequence of a small leak from the bottom section of the WD column. It is possible to reduce energy costs for WD by employing vapor recompression cycles between the reboiler and condenser, but this tends to increase complexity and capital cost, and is not recommended [43].

An electrolytic cell (**DE**) produces gas at the same molar tritium concentration as the feed water, averaged over a long period. The electrolyte gets enriched in tritium according to the separation factor, and hence presents a higher potential radiological hazard than the feed water. For a given concentration limit in the electrolyte (e.g. 100 [Ci/l]), light water processing is disadvantaged, since its maximum feed concentration is limited to about 20 % of a permissible heavy water concentration. The fact that tritium concentrates in the electrolyte rather than the product hydrogen is a disadvantage, since it creates a reservoir of high-tritium water that has no useful purpose. The electrolyte concentration can be reduced by providing an excess flow through the cell, but this in turn reduces the tritium concentration in the product hydrogen, increases the cell power requirement and increases the feed flow to the cryogenic unit. Tritium inventories are not appreciably reduced and the reduction in tritiated water concentration is not economically justified. The energy requirements for electrolysis are significant and not easily recoverable. Considerable tankage and peripheral equipment will be needed to maintain electrolyte conductivity and scrub electrolyte from the product hydrogen and oxygen. Electrolysis has been widely used for the production and upgrading of heavy water, including tritiated heavy water [43]. Currently, the most promising technology for future reactors seems to be the LPCE columns in CECE systems. Even if the system is more complex than for other options, the trade-off is size versus complexity. Principal Advantages and disadvantages of the previous technologies are summarized in Table 6.

Table 6 - Advantages and disadvantages of WDS technologies..

Technologies	Advantages	Disadvantages
CECE	Powerful capability for stripping tritium from water. Best options based on cost and minimum tritium inventory.	For large-scale application, CECE requires large electrolysis cells, and presents higher tritium concentration in the cells than in the rest of the process, due to separation factor. The issue of spent electrolyte waste and electrolyte replacement also is a disadvantage.
VPCE	Several years' operating experience.	Lower hydrogen inventory.
LPCE	System appears simpler, the process conditions are more benign.	The transfer efficiency is poorer.

2.3 Tritium permeation in plasma-facing and structural materials

Suppression of tritium permeation through structural materials is essential, in order to mitigate the fuel loss and to reduce radioactive safety hazards. Deuterium and tritium are all diatomic gases that dissociate, especially on metal surfaces, and dissolve into the metal lattice in their atomic form. The atoms readily recombine on the surfaces, resulting in permeation of the gaseous hydrogen isotopes through metals. If tritium is removed from the torus by the pumping system and sent to the reprocessing system, it is again filtered to separate it from other elements and separated from the other isotopes. All through the different steps, there is the potential for the tritium to permeate through the materials containing it, and for it to be released to the environment. With respect to tritium permeation, fusion reactor materials can be divided into two categories: plasma-facing materials and structural materials. Plasma-facing materials in future fusion devices will be heated by the high-energy neutrons, by direct interaction of the plasma particles, and by electromagnetic energy released from the plasma. Thus, plasma-facing materials must be refrigerated. Tritium losses can occur in the primary vacuum vessel primarily through the cooling tubes passing through the plasma-facing materials [44]. Tritium atoms have high mobility through high temperature structural materials, and the driving force of their permeation is characterized by the tritium partial pressure acting on a given material. Depending on the tritium partial pressures involved in the system, two possible extreme permeation models are available: diffusion-limited model and surface-limited model.

In the past many authors studied this net distinction between the two permeation regimes (e.g. [45], [46] and [47]) and they stated that for low tritium partial pressures the permeation is governed by surface limited model, whilst for high values the diffusion rules the mobility thought structural materials. When the system is characterized by low partial pressures, the diffusive model overestimates the permeated flux through a given wall, characterized by certain high and low pressures acting on it and a given temperature, with respective to the one estimated with surface-limited model. On the other hand, when the system is characterized by relatively high partial pressures, a surface–limited permeation model would overestimate the permeation flux through the same membrane at the same operative conditions. The threshold value dividing the low and the high pressure areas probably

depends on the operative conditions (e.g. structural materials, temperature, gas compositions, etc.). For example according to Ref. [48] this value has been stated to be around 10 [Pa], while in Ref. [49] this value is included between 100 and 1000 [Pa]. In case of Diffusion Limited Models (DLMs) (at relatively high pressures) hydrogen migration through the metal membrane is limited primarily by hydrogen diffusion in the metal lattice while the surface processes (hydrogen adsorption, desorption) are considerably faster [50]. On the other hand, when a Surface Limited Model (SLM) is assumed, the diffusion through the membrane occurs fast enough, so that any concentration gradient is cancelled by diffusion [51].

2.3.1 The physics of permeation

The tritium generated inside the lithium-lead domain permeate through the EUROFER wall to the water. There are also reversed flows, but their contributions are small compared with the previously. Inside the PbLi and inside the steel the hydrogen and tritium are present in atomic forms. Inside the water these elements are present in molecular forms, therefore recombination and dissociation processes (described below) happen in the interface between the EUROFER/Water. The hydrogen-isotope permeation through the material can be expressed in principle by a multiplication of two predominant processes: solution and diffusion [52]. When hydrogen is solved in the material as the atomic state, the hydrogen solubility c_{eq} [mol/m^3] is given by Sieverts' law:

$$c_{eq} = K_s p^{0.5} \tag{1}$$

where K_s is Sieverts' constant [mol/(m^3·Pa$^{0.5}$)] and p is the hydrogen pressure [Pa]. K_s and the hydrogen diffusivity D [m^2/s] are thermally activated processes expressed by the Arrhenius rate equation:

$$K_s = K_{s0} \exp\left(-\frac{E_s}{RT}\right) \tag{2}$$

$$D = D_0 \exp\left(-\frac{E_D}{RT}\right) \tag{3}$$

where E_s and E_D are the activation energies of solution and diffusion [J/mol], R is the gas constant, and T is the temperature [K]. Finally, the hydrogen permeation flux through the material at high pressure is given by Richardson's equation, obtained by combining permeating flux and Sieverts' law [53]:

$$J = \frac{DK_S}{d}(p_{high}^{1/2} - p_{low}^{1/2}) \tag{4}$$

where J is the permeation flux [mol/(m^{2}s)] inside the structure, D the diffusion coefficient in the material, K_S the Sievert's constant of the material, p the pressure [Pa] across the thickness d [m]. Both D and K_s depend strongly on temperature and have associated activation energies such that the permeation is much higher at high temperatures than at low. The $p^{1/2}$ dependence implies that the probability of incoming tritium atoms permeating

through the membrane decreases as pressure increases. Although this relationship applies adequately to a large variety of conditions, it often overestimates the permeation rate at low pressures.

Near the wall the following effects depend strongly on the tritium concentration in the surface and on the pressure.

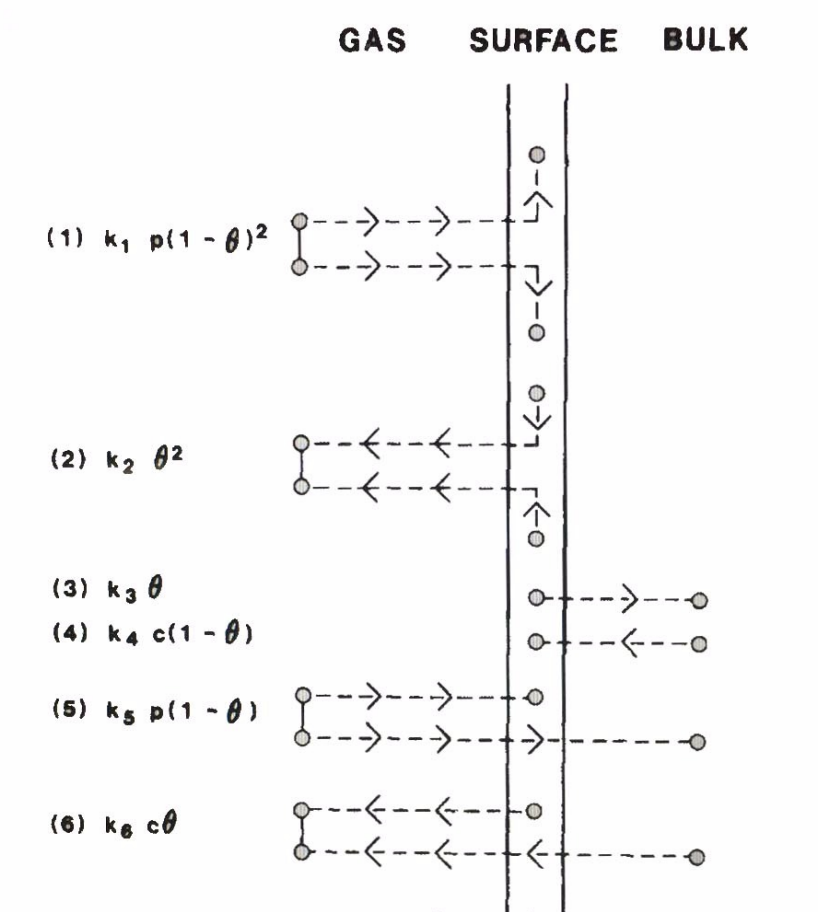

Figure 12 - Schematic diagram of the surfaces processes [54].

In Figure 12 the surfaces processes are represented. (1) A gas molecule strikes the surface, dissociates, and is adsorbed as two uncorrelated atoms, it's a dissociation processes. After disassociation at the surface, each atom thermalizes at a surface site before entering the bulk, since two sites are required, the probability for this is proportional to $(1-\theta)^2$ where θ is the fraction of surface sites already occupied. This process has an uptake rate at pressure p. (2) is the opposite processes, desorption, a pair of adsorbed atoms combine and evaporate as a molecule. (3) and (4) represent absorption of H atoms into the metal bulk and the reverse process which will be proportional to the bulk tritium atom concentration c just below the surface and the fraction of unoccupied surfaces sites $(1-\theta)$. In (5) a gas molecule strikes the surface and dissociates with one atom entering the bulk and the other adsorbed, the opposite is the (6) where a bulk atom jumps to the surface, combines with an adsorbed atom, and evaporates as a molecule.

The diffusion process of tritium through a metal membrane is ruled by Fick's equation.

$$\frac{\partial c}{\partial t} = D\frac{\partial^2 c}{\partial x^2} \tag{5}$$

that describes the time and the spatial development of the hydrogen concentration c in the time.

In permeation, there are mainly three phenomena:

Penetration: $$J_{in} = 2(\sigma K_s)p_T \tag{6}$$

Diffusion: $$J_D = -D\frac{\partial c}{\partial x} \tag{7}$$

Release: $$J_r = 2(\sigma K_r)_j c_j^2 \tag{8}$$

where the index j represent the different surfaces, σK_r and σK_s the surface constants for the release and for the solubilisation (σ is the surface roughness). (6) and (8) are surface processes, (7) it's a bulk processes.

The penetration rate J_{in}, is proportional to the driving tritium pressure p_T upstream; the factor 2 calculates molecules into atoms since all rates are given in [atoms/(cm^{2}s)].

In order to solve the Fick's law, the boundary conditions at the upstream (1) and downstream side (2) have to be taken into account:

$$J_{in} = 2(\sigma K_s)p_T = 2(\sigma K_r)_1 c_1^2 - D\frac{\partial c}{\partial x}\Big|_{x=x_1} \tag{9}$$

$$J_D = -D\frac{\partial c}{\partial x}\Big|_{x=x_2} = 2(\sigma K_r)_2 c_2^2 = J_P \tag{10}$$

The released flux density downstream correspond to the permeation flux density J_P.

Since $J_r \propto c_j^2$ an algebraic solution of the Fick's law cannot be found. In the steady state however, when the diffusion rate through a membrane of thickness x, becomes constant:

$$J_D = D\frac{c_1 - c_2}{x_0} \tag{11}$$

The above boundary conditions can be transformed into a general equation which is valid for any temperature and any material:

$$W^2 w^4 + 2\sqrt{\frac{\overline{\sigma K_r}}{(\sigma K_r)_1}}\, W w^3 + 2w^2 = 1 \tag{12}$$

where:

$$\overline{\sigma K_r} = \frac{2(\sigma K_r)_1(\sigma K_r)_2}{(\sigma K_r)_1 + (\sigma K_r)_2} \tag{13}$$

is an average of the two release rate constants.

$$w^2 = \frac{J_P}{J_{in}} \tag{14}$$

relates the permeation to the penetrating flux density, i.e. to the upstream pressure p_T.

$$W = \frac{J_{in}}{J_D} = \frac{2\sigma K_r}{D} cl \tag{15}$$

that represent the ratio of the penetrating and the diffusion rate called permeation parameter where l is the characteristic length of the c gradient near the surface [55].

In the case of $W \ll 1$ (corresponding to low p), the surface processes are determining; on the contrary when $W \gg 1$ (high p) the bulk processes are determining.

The equilibrium concentration, when the permeation flow is equal to that of release, is given by the Sieverts' law (eq.(1)) [54]. In the model a more general and intermediate treatment was used which includes both mass and surface phenomena.

2.4 Tritium permeation reduction barriers

The prevention of tritium losses by permeation through structures of a fusion reactor, such as the first wall, and breeder blanket containment is an important issue in fusion technology.

To guarantee adequate radiological protection of personnel and populations the design of the WCLL blanket for the DEMO fusion reactor required the deposition of permeation barriers on the cooling tubes and blanket module surface. A strong effort has been made in the past to select the best technological solution for the realization of Tritium Permeation Barriers (TPB). The best solution was identified in aluminum-rich coatings, which form Al_2O_3 at their surface [56]. The efficiency of the barrier is characterized by the permeation reduction factor (PRF), which is the ratio of permeation fluxes measured without and with the barrier.

$$PRF = \frac{J_{uncoated}}{J_{coated}} \tag{16}$$

An high permeation reduction factor $PRF > 10^2 - 10^3$.

2.4.1 Main requirements

Tritium barriers for a DEMO blanket configuration must satisfy several requirements in order to ensure an appropriate value of the Permeation Reduction Factor (PRF). These requirements are: chemical compatibility with the surrounding environment, with the PbLi alloy and with coolant (helium or water); compatibility with thermal loads, radiation and cyclic thermal stresses; compatibility with the structural material; self-healing (composite coating to address the problem of pores and cracks in ceramic coatings) in standard operating conditions.

The main problem with the permeation barriers is the deposition technique to adopt in order to obtain a uniform layer of oxide. Moreover, the coating properties strongly depend on the structural material. For this purpose, a thorough analysis must be carried out.
Tritium barriers appear mandatory, to satisfy fusion nuclear technology issues in many design options, especially for certain blanket options. On the other hand, barriers can potentially increase the degradation of structural materials due to their immobilization of hydrogen. In many designs, it is desirable to reduce the permeation rate by a factor of over 1000 in comparison to the bare metal.

Barriers based upon aluminum (and titanium to a lesser extent) have been demonstrated to provide permeation reduction factors from 1.000 to 1.000.000 in laboratory situations [57]. The rate-controlling mechanism may actually be associated with the character and population of defects, rather than the intrinsic character of the surface coatings. Coatings appear to be relatively robust.

In-reactor testing has not been able to retain the same properties measured in laboratory. The lower PRFs in irradiation testing may be associated with radiation-induced diffusion (RID) of hydrogen, based upon ionization of the transporting species and some corrosion effects.

With no completely satisfactory barrier system actually available, it is necessary to continue both fundamental research and engineering demonstration of new barrier systems, in order to solve this problem. A better understanding of the migration mechanism of hydrogen isotopes through these barriers is required, including irradiation effects [58].

2.4.2 Technologies for PRF

Several fabrication approaches for preparing Al_2O_3 coating have been developed, including hot-dip (HD) aluminization process developed by FZK, chemical vapor deposition (CVD) process developed on laboratory scale by CEA, vacuum plasma spray (VPS), detonation jet, low pressure plasma spray (LPPS) and air plasma spray (APS) [59].

Fe–Cr–Al alloys have been also considered a suitable coating for the RAFM steels: a thin layer of dense, self-healing and adherent Al_2O_3 forms on the surface upon oxidation in PbLi alloy. Fe–Cr–Al alloys are extremely oxidation resistant even at such a high temperature as 1100 [°C], benefiting from the formation of Al_2O_3 film.
Fe–Cr–Al alloy foils (JFE, Japan) with a thickness of 50 [μm] and chemical composition of Fe–20Cr–5.5Al–0.1Mn–0.08La (wt.%) were employed as substrates on which Al_2O_3 coatings were prepared.

Pure Al_2O_3 coatings on a Fe–Cr–Al alloy as a potential tritium permeation barrier were fabricated on both fresh and pre-oxidized surfaces by sol–gel method, and some conclusions driven. In particular, the thermally grown and sol–gel prepared coatings are somewhat porous on the top surface; however dense in depth. With increase in temperature from 500 to 1100 [°C], at which the coating is thermally calcined, the crystal structure of the sol–gel prepared Al_2O_3 coating changes from amorphous to γ-Al_2O_3 and then to α-Al_2O_3. The thermally grown and sol–gel prepared coatings are uniform in thickness, crack-free and well adhered to the substrates, which suggests that such prepared coatings may be effective on preventing tritium permeation. This needs to be experimentally confirmed [60].

3 Tritium transport in the WCLL breeding blanket

3.1 Why study tritium transport?

The study of tritium transport in blankets is fundamental to assess their preliminary design and safety features [61] [62]. Tritium permeation through Breeding Blanket is a crucial aspect for the design of the next generation DEMO fusion power plants. Tritium is generated inside the breeder, dissolves in and permeates through materials, thus leading to a potential hazard for the environment. For this reason, it is important to carry out tritium migration analyses for each DEMO blanket configuration, in order to predict the released amount of tritium during the plant operation [63]. Knowing the evolution of tritium amount allows to reduce fuel leakage from the fusion reactor too.

3.2 The mathematical model

The macroscopic behavior of fluids is the same as if they were perfectly continuous; physical quantities such as mass and momentum associated with the matter contained within a given small volume will be considered to be spread uniformly over that volume, instead actually concentrated in a small fraction of it. There is sufficient observational evidence that the common real fluids, both gases and liquids, move as if they were continuous, but some of the properties of the equivalent continuous media need to be empirically determined.

Eulerian method and Lagrangian method can be used to study the dynamics of continuous systems at microscopic level. The Eulerian method describes the time evolution of macroscopic quantities such as velocity, density and pressure at a given point, by means of space-independent spatial derivatives. The Lagrangian method describes instead the variables time behavior following the trajectories of fluid elements: the Lagrangian derivative also takes into account the motion of the fluid. In the laminar regime, the fluid flow can be completely predicted by solving Navier-Stokes equations, which give the velocity and the pressure fields. Let us first assume that the velocity field does not vary with time.

As the flow begins to transition to turbulence, oscillations appear in the flow, despite the fact that the inlet flow rate does not vary with time. It is then no longer possible to assume that the flow is constant. In this case, it is necessary to solve the time-dependent Navier-Stokes equations, and the mesh used must be fine enough to resolve the size of the smallest eddies in the flow.

A computational thermal and fluid-dynamic model has been developed to investigate the thermal-hydraulic efficiency of the WCLL breeding blanket, to evaluate the temperature

distribution in the structures and the thermal field and flow path in the breeding zone. Simulations results highlight where allowable limits are not met. Possible criticalities in the PbLi flow paths (i.e. stagnant or low flow zone near the tubes and baffle) are identified, giving hints for enhancements of baffle plate geometry and for the layout of the tubes in the breeding zone. In this case, the model permits to determine the temperatures in the blanket different zones, to be implemented in a second model for tritium transport study.

The 2015 design of the WCLL BB has been considered for the development of this model [64]. The tokamak is divided into 18 equal toroidal sectors: each sector is made of three identical OB and two identical IB segments; each segment contains 7 Breeding Modules (BMs). Each BM, includes a portion of the FW and BZ containing the PbLi breeder material. The cooling circuit is split when entering the vessel, with two different sets of manifolds delivering the water coolant to the FW and the BZ in parallel [65].

The FW loop, it is formed by rectangular cooling channels immersed in the FW solid structure.

The BZ part is cooled by circular double-wall tubes, which are in contact with the PbLi flowing in the free space on their outer side. The tubes are arranged in a modular layout, with a set of elementary cells of 21 tubes ideally stacked in the poloidal direction. In the model, the coaxial tubes were considered as a single tube with a thickness given by the sum of the two.

3.2.1 Laminar flow

The PbLi laminar motion has been analyzed within its channel. The low input speed does not create turbulence; then, Navier-Stokes equations are sufficient to solve the motion of incompatible fluid. The density and viscosity of the PbLi have been taken from the material database. When the temperature variations in a flow are small, a single-phase fluid can often be assumed incompressible; that is, ρ is constant or nearly constant. This is the case for all liquids under normal conditions and for gases at low velocities too. For constant ρ, the incompressible formulation of the continuity reduces to:

$$\rho \nabla \cdot (\boldsymbol{u}) = 0 \tag{17}$$

and the momentum equation becomes:

$$\rho(\boldsymbol{u} \cdot \nabla)\mathbf{u} = \nabla[-p\boldsymbol{I} + \mu(\nabla \boldsymbol{u} + (\nabla \boldsymbol{u})^T)] \tag{18}$$

where: ρ is the denstity [kg/m^3], $\boldsymbol{u}$ is the velocity vector [m/s], p is the pressure [Pa], μ the dynamic viscosity [Pa·s].
The initial PbLi values are set at 1.1 [mm/s] for the inlet velocity and $5 \cdot 10^5$ [Pa] for the inlet pressure [1].

Fundamental to the analysis of fluid flow is the Reynolds number:

$$Re = \frac{\rho U L}{\mu} \tag{19}$$

where U denotes a velocity scale, and L denotes a representative length; in this case the radial length and the PbLi velocity. The Reynolds number represents the ratio between inertial and viscous forces. At low Reynolds numbers, viscous forces dominate and tend to damp out all disturbances, which leads to laminar flow. At high Reynolds numbers, the damping in the system is very low, giving to small disturbances the possibility to grow due to nonlinear interactions. With the data present in Table 7 was obtained a Reynolds number of 490, characteristic of a laminar flow.

Table 7 - Data for Raynolds number at 598 [K]

Data	Value	U.o.M.
U	1.01	[mm/s]
L	0.096	[m]
ρ	9808.3	[kg/m^3]
μ	$1.94 \cdot 10^{-3}$	[Pa·s]

3.2.2 Heat transfer

Heat transfer equations have been used in the model too, to know the temperatures within the elementary cell that will then be used in the transport model of diluted species. Heat transfer is defined as the flow of energy due to a difference in temperature. It deals with conduction, convection and radiation mechanisms.

A separate study was conducted on the turbulent motion of water within the tubes. The high pressure that characterizes the flow of the coolant, in the toroidal direction, causes a small temperature variation that they can be neglected. The same can be said for pressure drops in the toroidal direction which are negligible in 0.234 [m] of tube length. A constant value of pressure and temperature was then chosen and introduced in the final model, in order to lighten the computational cost.

The fundamental law governing all heat transfer is the first law of thermodynamics, commonly referred to as the principle of conservation of energy. However, internal energy, U, is a rather inconvenient quantity to measure and use in simulations. Therefore, the basic law is usually rewritten in terms of temperature, T. For a fluid, the resulting heat equation is:

$$\rho c_p \boldsymbol{u} \cdot \nabla T = \nabla \cdot (k \nabla T) + Q \tag{20}$$

the Heat Transfer interface with the Heat Transfer in Fluids feature of Comsol solves this equation for the temperature, T. Where: ρ is the density, c_p the fluid heat capacity at constant pressure, k the fluid thermal conductivity, $\boldsymbol{u}$ the fluid velocity field, Q the heat source (or sink).

3.2.3 Tritium transport

The last step is tritium transport. In particular, the transport of diluted species is considered, as the final purpose of this analysis.

The transport of diluted species approach assumes chemical species transport through diffusion and convection and implements the mass balance equation as:

$$\frac{\partial c}{\partial t} + \boldsymbol{u} \cdot \nabla c = \nabla \cdot (D \nabla c) + s \tag{21}$$

where: c is the concentration of the species [mol/m^3], D denotes the diffusion coefficient [m^2/s], s is a reaction rate expression for the species [mol/(m^3·s)], $\boldsymbol{u}$ is the velocity vector [m/s].

The first term on the left-hand side of equation (21) corresponds to the accumulation (or indeed consumption) of the species. The second term accounts for the convective transport due to a velocity field u. This field is obtained from coupling this physics interface to one that describes fluid flow (momentum balance). On the right-hand side of the mass balance equation, the first term describes the diffusion transport, accounting for interaction between the dilute species and the solvent. Finally, the second term on the right-hand side represents a source or sink term, typically due to a chemical reaction.

3.3 Boundary Conditions

In the previous section the various physics implemented in COMSOL model were illustrated; it is now necessary to define the boundary conditions to proceed with the model solution.

3.3.1 Heat transfer B.C.

The heat equation accepts two basic types of boundary conditions: specified temperature and specified heat flux. The former is constraint-type, and sets the temperature at a boundary (Dirichlet B.C.) as:

$$T = T_0 \tag{22}$$

while the latter specifies the inward heat flux:

$$-\boldsymbol{n} \cdot \boldsymbol{q} = q_0 \tag{23}$$

where: $\boldsymbol{q}$ is the conductive heat flux vector $\boldsymbol{q} = -k\nabla T$ [W/m^2], $\boldsymbol{n}$ is the normal vector of the boundary, q_0 is inward heat flux [W/m^2], normal to the boundary [66].
The inward heat flux, q_0, is often a sum of contributions from different heat transfer processes (for example, radiation and convection). For tungsten this value has been imposed equal to $0.5 \cdot 10^6$ [W/m^2].

The special case $q_0 = 0$ is called thermal insulation (Neumann B.C.) and - in this case - it has been applied to all boundaries of the elementary cell taken into consideration, except for the FW where the flow q_0 was imposed. This condition specifies where the domain is a well-insulated one. Intuitively, this equation states that the temperature gradient across the boundary must be zero. For this to be true, the temperature on one side of the boundary must equal the temperature on the other side. Because there is no temperature difference across the boundary, heat cannot transfer across it.

The outflow node provides a suitable boundary condition for convection-dominated heat transfer at outlet boundaries. It has been applied to both the flow of water and of PbLi. In a model with convective heat transfer, this condition states that the only heat transfer over a boundary is by convection. The temperature gradient in the normal direction is zero, and there is no radiation. This is a good approximation of the conditions at an outlet boundary in a heat transfer model with fluid flow.
An input temperature for PbLi and water was also set; the equation for this condition is $T = T_0$ where T_0 is the prescribed temperature on the boundary (598.15 [K] for PbLi and 558.15 [K] for water).

3.3.2 Laminar flow B.C.

Navier-Stokes equations can show a wide variety of numerical behaviors ranging from almost completely elliptic to almost completely hyperbolic [67]. This has implications when it comes to prescribing admissible boundary conditions. There is also a discrepancy between mathematically valid boundary conditions and practically useful boundary conditions.

An inlet requires specification of the velocity field components, the most robust way to do this is to set a velocity field. A common alternative to prescribing the complete velocity field is to prescribe a pressure, in which case the normal velocity component will be specified indirectly via the continuity equation. The pressure can be assumed to be pointwise, which is – from the mathematical viewpoint - an over-constraining but a numerically robust formulation. Alternatively, the pressure can be specified via a stress condition:

$$-p + \mu \frac{\partial u_n}{\partial n} = F_n \tag{24}$$

where $\partial u_n / \partial n$ is the normal derivative of the normal velocity field component.

Setting a pressure value is the most common boundary condition approach at the outlet. As in the case of inlets, the pressure can be specified either pointwise or via a stress condition.

Specifying the pressure only is however mathematically not sufficient, unless the Reynolds number is infinity. In practice, it can be enough if the Reynolds number is high enough. Otherwise, the pressure boundary condition must be supplemented by conditions on the tangential velocity components. This is often achieved by setting a vanishing tangential stress:

$$\mu \frac{\partial u_t}{\partial n} = 0 \tag{25}$$

where $\partial u_t / \partial n$ is the normal derivative of the tangential velocity field. It is also possible to prescribe u_t to be zero. The latter option should be used with care since it can have a significant effect on the upstream solution [68].

The elliptic characteristic of the Navier-Stokes equations permit mathematically a complete velocity field to be specified on an outlet. This can however be difficult to apply in practice. The reason is that it's hard to specify the outlet velocities so that they are consistent with the interior solution at each point. The adjustment to the specified velocity will then occur across an outlet boundary layer. The boundary layer thickness will depend on the Reynolds number: the higher the Reynolds number, the thinner the boundary layer.

The total stress on the boundary is set equal to a stress vector of magnitude f_0, oriented in the negative normal direction (incompressible formulation):

$$\left(-p\boldsymbol{I} + \mu(\nabla \boldsymbol{u} + (\nabla \boldsymbol{u})^T)\right)\boldsymbol{n} = -f_0 \boldsymbol{n} \tag{26}$$

This implies that the total stress in the tangential direction is zero. This boundary condition implicitly sets a constraint on the pressure that for 2D flows is:

$$p = 2\mu \frac{\partial u_n}{\partial n} + f_0 \tag{27}$$

If $\partial u_n / \partial n$ is small, then $p \approx f_0$. In this case, the pressure at the output of the PbLi channel was set to 0 [Pa].

The wall includes a boundary condition describing the fluid flow condition at a wall. The default boundary condition for a stationary solid wall is the "no slip" one. The condition prescribes $\boldsymbol{u} = 0$, that is, the fluid at the wall is not moving; this boundary has been applied across the entire PbLi domain. At the inlet, velocity field is selected. The velocity is set equal to a given velocity vector u_0 when $u_x = u_0 = 1.1$ [mm/s] (PbLi), $u_y = u_z = 0$. Two outlet boundary conditions have been implemented for the pressure (one for BZ and one for FW) $p_0 = 155\ [bar]$.

Finally, the boundary conditions for the transport of diluted species were introduced.

3.3.3 Tritium transport B.C.

The last boundary conditions to be analyzed concern the most complex model in this work from the physics viewpoint: the transport of tritium. The species equations require an initial value for the concentration of species assumed as:

$$c_{i,0} = 0 \tag{28}$$

[mol/m^3] both for water concentration, EUROFER and PbLi. Transport of Diluted Species was linked with the Surface Reaction by a Flux defined in the wall of the channel according to the following equation:

$$-\boldsymbol{n}(J_{i,1} - J_{i,2}) = J_{0,i} \tag{29}$$

with J [mol/(m^2·s)].
The dissociation and recombination phenomena take place at the Water/EUROFER interface. There is a molecular flow in the water side defined taking into account both effects:

$$\left(-D_{T_2,w}\nabla c_3 + c_3 \cdot \vec{u}\right) \cdot \hat{n}|_{W/Eu} = \; - k_d \cdot p_{T_2,w} + k_r \cdot c_2^2 \tag{30}$$

$$\left(-D_{T,Eu}\nabla c_2\right) \cdot \hat{n}|_{Eu/W} = \; 2 \cdot (k_d \cdot \frac{c_3}{k_H} - k_r \cdot c_2^2) \tag{31}$$

Equation (30-31) bear - in the left hand terms - the molecular flows in the water side ([mol/m^3]) and in EUROFER side of the interface. The positive direction of the flow has been chosen from the material to the water pipe, while k_d is the dissociation coefficient [mol/(m^2 s Pa)], k_r is the recombination coefficient [m^4/(mol s)], and k_H is the Henry constant [mol/(m^{3}Pa)], obtained dividing the partial pressure of the corresponding gas by the concentration c. The output conditions for the flow have been set equal to zero.

The right hand term of equation (30) was entered into COMSOL as the incoming flow [mol/(m^2 ·s)] in the transport of diluted species at the interface EUROFER/water (eq. (32)), while that of equation (31) as PDE on the boundary:

$$e_\alpha \frac{\partial^2 c_s}{\partial t^2} + d_\alpha \frac{\partial c_s}{\partial t} + \nabla \cdot \Gamma = f \tag{32}$$

To ensure mass conservation e_α is the mass coefficient set equal to zero, d_α is a damping coefficient set equal to 1, $\Gamma = -c_{s,tx} \cdot D$, $\Gamma = -c_{s,ty} \cdot D$ and $\Gamma = -c_{s,tz} \cdot D$ are the conservative flux vector [mol/(m·s)], $c_{s,t}$ refer to the components of the gradient. f is the source term [mol/(m^2·s)], c_s is the default field and variable name for a single scalar PDE variable; in this case, it is a surface concentration [mol/m^2] and the main output value of the PDE.

In the interface PbLi/Eurofer the tritium is present in its atomic form. As a consequence, there is no recombination nor dissociation at this interface. The continuity of the partial pressure of tritium is given by:

$$c_2 = \frac{k_{s,Eu}}{k_{s,LM}} \cdot c_1 = K_j \cdot c_1 \tag{33}$$

where: c_1 and c_2 are the tritium concentrations [mol/m^3] in PbLi and Eurofer, $k_{s,Eu}$ and $k_{s,LM}$ are the Sieverts' constant of the materials at both sides of the interface, j refers to hSPs,

baffle or pipes.

The resolution of the equation system starts from the stationary solution of a multi-physics model that combines the equation of heat transfer within the entire elementary cell and the Navier-Stokes equations of mass and momentum conservation. The results obtained from the heat transfer and laminar flow were used as input for the resolution of the GTE; thanks to the resolution algorithm it has thus moved from a fully coupled system to a weakly coupled system. Iterations were subsequently performed until an error of less than 10% was obtained. The flow chart is shown in Figure 13. The summary of the boundary and initial conditions are present in Table 8.

ICs have been set regarding the initial temperatures of water, PbLi, and EUROFER, the last one has been set equal to the initial temperature of the PbLi. Velocity and pressure for the turbulent motion of the water have been considered constant since their variation in the toroidal direction is almost zero. A heat flux [W/m^2] was also set on the FW and three different heat sources [W/m^3] on the water, PbLi and EUROFER domains.

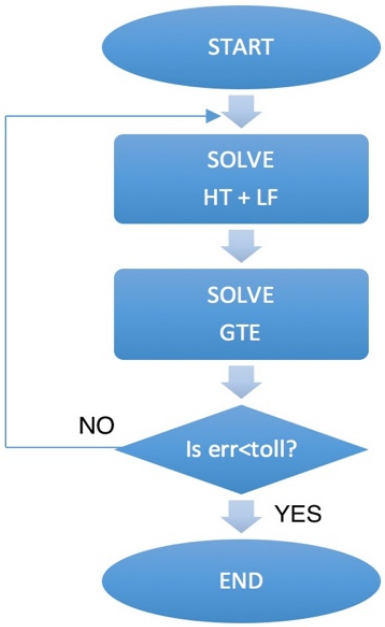

Figure 13 - Flow chart.

Table 8 -Summary of the boundary and initial conditions

BOUNDARY CONDITIONS			
Type	**Location**	**Equation**	**Values**
		Heat Transfer	
Temperature inlet	PbLi inlet	$T = T_{LM}$	$T_{LM} = 325\ [°C]$
Temperature inlet	Water FW inlet	$T = T_{W,FW}$	$T_{W,FW} = 285\ [°C]$
Temperature inlet	Water BZ inlet	$T = T_{W,BZ}$	$T_{W,BZ} = 285\ [°C]$
Heat flux	On Tungsten (FW)	$-\boldsymbol{n} \cdot \boldsymbol{q} = \boldsymbol{q_W}$	$\boldsymbol{q_W} = 0.5{\cdot}10^6 [W/m^2]$
Out Flow	Water FW outlet	$-\boldsymbol{n} \cdot \boldsymbol{q} = 0$	
Out Flow	Water BZ outlet	$-\boldsymbol{n} \cdot \boldsymbol{q} = 0$	
Out Flow	PbLi Outlet	$-\boldsymbol{n} \cdot \boldsymbol{q} = 0$	
		Laminar Flow	
No slip	PbLi/EUROFER surface	$\boldsymbol{u} = 0$	
Inlet velocity	PbLi inlet	$\boldsymbol{u} = -v_{LM}$	$v_{LM} = 1.01\ [mm/s]$
		Transport od Diluted Species	
No Flux	PbLi boundary	$-\boldsymbol{n} \cdot \boldsymbol{N}_i = 0$	
No Flux	EUROFER boundary	$-\boldsymbol{n} \cdot \boldsymbol{N}_i = 0$	
Flux	EUROFER/Water interface	$-\boldsymbol{n} \cdot \boldsymbol{N}_i = 2 \cdot J_{perm}$	
Outflow	Water BZ	$-\boldsymbol{n} \cdot D\nabla c = 0$	
Outflow	PbLi	$-\boldsymbol{n} \cdot D\nabla c = 0$	
Inflow	Water BZ	$c = 0$	
Inflow	PbLi	$c = 0$	
		INITIAL CONDITIONS	
EUROFER concentration	EUROFER	$c = 0$	
Water BZ concentration	Water BZ	$c = 0$	
PbLi concentration	PbLi	$c = 0$	

3.4 Input data

3.4.1 Materials properties

Operating conditions for most fusion materials are quite demanding: for instance, materials in components close to the plasma - such as first wall, breeding blanket and divertor - must withstand high radiation levels, high transmutation rates, high temperatures and high thermo-mechanical stresses.

These extreme conditions make the development and characterization of plasma facing and structural materials very important topics for design and application, both at experimental and reactor levels. Good physical and mechanical properties, such as good creep strength and fatigue resistance, minimum embrittlement due to transmutation products, corrosion resistance and low neutron-induced activation are necessary. In this case, EUROFER97 steel is considered as a structural material for the blanket modules. EUROFER97 is the outcome of a joint effort of the European Union to develop a low activation steel, to be used not in direct contact with the fusion reactions but as a second shielding. EUROFER97 has an operating temperature in the range 620 – 820 [K], the lower limit being due to irradiation embrittlement and the higher limit due to creep-fatigue strength.

Tungsten has been chosen as the plasma-facing material. Tungsten and tungsten-based materials are considered as top candidates for various fusion applications due to their

excellent high-temperature properties. They combine a high melting point, high creep resistance, high temperature strength, good thermal conductivity, low vapor pressure and good erosion resistance. However, in contrast to these excellent high-temperature properties, brittleness at low temperatures is the main disadvantage of the proposed material. W, like most body-centered cubic (bcc) metals, has a characteristic transition from brittle to ductile behavior, taking place at a certain temperature. An exact value of the transition temperature cannot be given, as this quantity strongly depends on the material's condition (i.e. microstructure and testing direction) [69] and on the strain-rate.

Coolant is water at typical PWR conditions: pressure 155 [bar], inlet temperature 285 [°C] and outlet temperature 325 [°C]. The thermodynamic properties of the PbLi and EUROFER, used in the calculation, are shown in Tab. 9. Tungsten and water properties from the COMSOL Multiphysics library were used.

Table 9 - Thermodynamic properties of EUROFER and PbLi.

		EUROFER [70]
Density	$[kg/m^3]$	$7819 - 0.2018 \cdot T - 1.112 \cdot 10^{-4} \cdot T^2$
Specific Heat	$[J/Kg/K]$	$2.696 \cdot T\ [K] - 4.69 \cdot 10^{-3} \cdot T^2\ [K] + 3.335 \cdot 10^{-6} \cdot T^3\ [K]$
Thermal Conductivity	$[W/m/K]$	$5.4308 + 0.13565 \cdot T\ [K] - 0.00023862 \cdot T^2\ [K] + 1.3393 \cdot 10^{-7} \cdot T^3\ [K]$
		PbLi [71]
Density	$[kg/m^3]$	$10520.35 - 1.19051 \cdot T[K]$
Specific Heat	$[J/Kg/K]$	$195 - 9.116 \cdot 10^{-3} \cdot T\ [K]$
Thermal Conductivity	$[W/m/K]$	$(14.51 + 1.96 \cdot 10^{-2} \cdot T\ [K]$
Dynamic Viscosity	$[Pa \cdot s]$	$1.87 \cdot 10^{-4} \cdot exp\left(\frac{11640}{R \cdot T\ [K]}\right)$
Vol. th. Expansion Coeff.	$[1/K]$	$1.124 \cdot 10^{-4} + 1.505 \cdot 10^{-8} \cdot T$ [K]

3.4.2 Physical and transport properties

3.4.2.1 Tritium solubility

The determination of the tritium inventory within the blanket and its environmental release requires the hydrogen ionization in lithium lead, which is defined by hydrogen Sievert's constant (Tab. 10). The tritium Sieverts' constant in PbLi has a great impact on the assessment of tritium losses, that can vary by more than one order of magnitude [72].

A weak point of PbLi is the low value of the tritium solubility constant that results in a high tritium permeation rate from the liquid metal to the primary cooling system, at least in absence of efficient tritium permeation barriers. In particular, the determination of tritium solubility in PbLi is of basic importance, since it directly affects all functional properties of the blanket. In particular, tritium inventory, permeation rate, and extraction efficiency are affected by its solubility in PbLi [73]. In case of hydrogen atoms dissolved in metals (i.e.,

the case for tritium in PbLi and blanket structural materials), the tritium solubility can be defined by means of the Sievert's law, as already shown (eq.(1)).

The solubility represents equilibrium between the diatomic tritium molecule and tritium atoms in a metal according to the following reaction [74]:

$$\frac{1}{2}T_2 \leftrightarrow T \tag{34}$$

It is important to distinguish between solubility and concentration: the solubility is a thermodynamic property of the material, while the concentration is a variable that depends upon system conditions. For example, once dissolved in a metal lattice, atomic tritium can interact with elastic stress fields: hydrostatic tension dilates the lattice and increases the concentration of tritium that can dissolve in the metal, while hydrostatic compression decreases the concentration.

On the other hand, internal stresses near defects or other stress concentrators can substantially increase the local concentration near the defect. While it is unlikely that local concentrations would significantly contribute to a higher tritium inventory in the whole material, nevertheless locally elevated concentrations of hydrogen isotopes can become sites for initiating and propagating hydrogen-assisted fracture in structural metals.

Table 10 - Data for tritium solubility.

	U.o.M.		Ref.
$K_{s\|EUROFER}$	$[mol/m^3/Pa^{0.5}]$	$1.02 \cdot 10^{-1} \cdot \exp\left(\frac{-23810}{RT}\right)$	[75]
$K_{s\|PbLi}$	$[mol/m^3/Pa^{0.5}]$	$1.25 \cdot 10^{-3} \cdot \exp\left(\frac{-1350}{RT}\right)$	[75]

3.4.2.2 Tritium diffusivity

Tritium diffusion in metals is simply the process of atomic tritium moving or hopping through a crystal lattice. Tritium tends to diffuse quite rapidly through most materials and its diffusion can be measured at relatively low temperatures. The diffusivity D is a thermodynamic parameter; therefore, it follows the conventional Arrhenius-type dependence on temperature:

$$D = D_0 \exp\left(\frac{-E_D}{RT}\right) \tag{35}$$

where D_0 is a constant and E_D is the activation energy of diffusion. Measuring tritium diffusion is a non-trivial task, due to the limited availability of tritium, and its radiological hazard. Thus, hydrogen and deuterium are often used as surrogates. From classic rate theory, it can infer that the ratio of diffusivity of hydrogen isotopes is equivalent to the inverse ratio of the square root of the masses of the isotopes [44]:

$$\frac{D_T}{D_H} = \sqrt{\frac{m_H}{m_T}} \tag{36}$$

While this equation provides a first good estimate of the relative diffusivity of hydrogen and its isotopes, more advanced theories have been applied to explain experimental data; for example, quantum corrections and harmonic effects can account for discrepancies between experimental and theoretical values of diffusivity [76] [77]. Table 11 shows the main parameters used for our tritium transport analysis.

Table 11 - Data for tritium diffusivity.

	U.o.M.		Ref.
$D\|_{T\text{-EUROFER}}$	$[m^2/s]$	$1.22 \cdot 10^{-7} \cdot \exp\left(\frac{-14470}{RT}\right)$	[75]
$D\|_{T\text{-Water}}$	$[m^2/s]$	$\frac{k_B \cdot T_w}{6\pi \cdot \mu_w \cdot r}$	[78]
		$7.4 \cdot 10^{-15} \frac{T_w \sqrt{\beta M_w}}{\mu_w \cdot v_T^{0.6}}$	
$D\|_{T\text{-PbLi}}$	$[m^2/s]$	$4.03 \cdot 10^{-8} \cdot \exp\left(\frac{-19500}{RT}\right)$	[79]
K_d	$[mol/m^2/s/Pa]$	$2.998 \cdot 10^{-8} \cdot \exp\left(\frac{-29230}{RT}\right)$	[80] [81]
K_r	$[m^4/mol/s]$	$2.838 \cdot 10^{-7} \cdot \exp\left(\frac{28679}{RT}\right)$	[80] [81]

K_B is the Boltzmann's constant; T_w is the water temperature [K]; μ_w is the dynamic viscosity of water [Pa s]; r is the Van Der Waals radius of hydrogen; β is an empirical coefficient equal to 2.6; M_w is the solvent molar mass [g/mol]; v_T is the molar volume of tritium.

3.4.3 Henry's constant

Henry's law is used to describe the solubility of gases in liquids. Henry's constant typically increases with temperature, passes through a maximum and then decreases at higher temperatures.

According to Harvey [82], the constant for high temperature ranges was calculated.

$$\ln K_H = \ln P_1^s + \frac{A}{T^*} + \frac{B(1-T^*)^{0.355}}{T} + f(C, T^*) \tag{37}$$

expressed in [1/MPa] where was used the reduced temperature:

$$T^* = \frac{T}{T_{c,1}} \tag{38}$$

$T_{c,1} = 647$ [K] is the solvent's critical temperature, A, B, C are parameters for correlations that for H_2 solute they are worth: $A = -4.4964 \;\; B = 6.0952 \;\; C = 5.8390$. The last term of equation (42) has an arbitrary form, it is set as a function of the temperature only:

$$f(C;T^*) = C\exp(1-T^*)\,(T^*)^{-0.41} \tag{39}$$

P_1^S represents the solvent vapor pressure, function of the temperature end calculated thanks to the work of Saul-Wagner (1987).

$$\ln\left(\frac{P_1^S}{P_C}\right) = \frac{T_c}{T}\left[a_1\tau + a_2\tau^{1.5} + a_3\tau^3 + a_4\tau^{3.5} + a_5\tau^4 + a_6\tau^{7.5}\right] \tag{40}$$

where $T_c = 647$ [K] and $P_C = 22$ [MPa] are reference constants and

$$\tau = 1 - \frac{T}{T_c} \tag{41}$$

with:

$a_1 = -7.85951783$	$a_4 = 22.6807411$
$a_2 = 1.84408259$	$a_5 = -15.9618719$
$a_3 = -11.7866497$	$a_6 = 1.80122502$

By replacing the value obtained in equation (40) in equation (37), gives a value for the Henry constant equal to: $K_H = 3.76146 \cdot 10^{-5}$ [mol/(m^{3}Pa)].

3.4.4 Tritium generation rate inside the lithium-lead

PbLi is a very attractive material for a breeding blanket, since it can lead to tritium self-sufficiency, it is not prone to irradiation damage and, compared with ceramic breeders, has high thermal conductivity. A weak point of PbLi is its low tritium solubility, that results in a high tritium permeation rate from the liquid metal to the primary cooling system, at least in absence of efficient tritium permeation barriers. In particular, the determination of tritium solubility in PbLi is important, since it directly affects all functional properties of the blanket, particularly in the determination of tritium inventory, tritium permeation rate, and tritium extraction efficiency.

Tritium inventories can be built in different stages of the tritium cycle, depending on the time constants of the different processes and loops (e.g., diffusion processes in the breeding materials) or by trapping mechanisms. A general issue is to minimize the tritium inventory in the different parts of the reactor (in the VV as well in the tritium plant); this is a safety concern related to possible mobilization of these inventories in case of an accident and its release in the environment. For this reason, the tritium cycles must be optimized, to reduce time constants in the tritium processes and then minimize the inventories.

Future fusion reactors are based on the fusion of deuterium and tritium nuclei which yields 14.1 [MeV] neutrons and 3.5 [MeV] alpha particles. A reactor with a fusion power of 500 [MW] (ITER) would need to fuse about 1.78×10^{20} T [nuclei/s] which is equivalent to 0.885 [mg] tritium per second or 76 [g] tritium per day. Since only a small fraction of the tritium of the order of 1% is burnt up in the fusion reaction, the residual tritium - together with the fusion product ^{4}He and further impurities - needs to be pumped out of the plasma chamber for fuel cleanup and reuse. To achieve this goal, a closed tritium fuel cycle (inner fuel cycle) is necessary. Future fusion reactors as DEMO with 2.7 [GW] fusion power will need more than 100 [kg] tritium per year so that tritium will have to be produced directly inside the fusion machine.
Table 12 illustrates the production and consumption of future reactors.

Table 12 - Tritium key parameters for ITER and DEMO [83].

		ITER	DEMO
Fusion power	[GW]	0.5	2.7
T consumption, full power day	[g/d]	76	412
T production, full power day	[g/d]	<0.4	~450

The tritium generation rate [mol/(cm^{3}s)] imposed on the elementary cell is shown in Figure 14. HCLL data are used [61], as the calculations on the radial neutron distribution of the BU of the WCLL have not been performed yet [84].

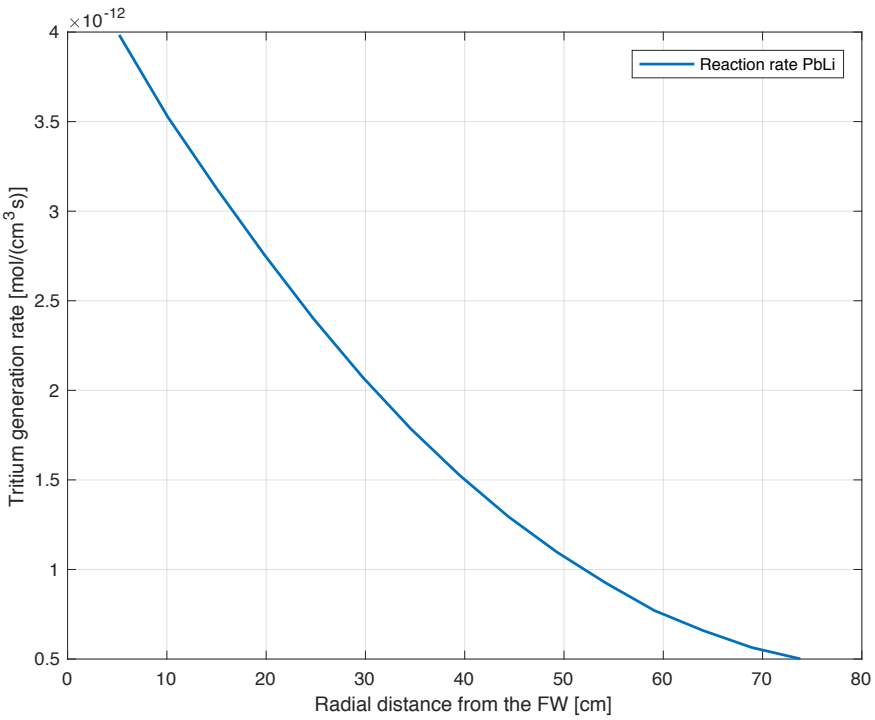

Figure 14 - Reaction rate PbLi [84].

3.4.5 Volumetric thermal heat flux

Two main sources of heating affect in-vessel systems: first, a volumetric source caused essentially by neutrons coming from the plasma core, then a surface heating generated by the plasma edge and collected by the surfaces of the plasma-facing components. The volumetric heat deposition is due to neutrons, which carry 80% of the fusion power. Neutrons have an initial kinetic energy of 14 [MeV], and are generated in the plasma D-T reactions.

This quantity is expressed in terms of a power per unit volume [MW/m^3] and can be used to get a quantitative measure of the intensity of this power flux in different parts of the machine. The Neutron Wall Loading (NWL), instead, is expressed in [MW/m^2] terms, being the energy per unit time of the incoming neutron current at the first wall surface unit.

The second thermal source is localized at the surface of the components facing the plasma (FW). This power derives from the remaining 20% D-T fusion power that is associated to the alpha particles with the addition of the heating directly injected into the plasma (i.e., heating and current driver systems). Several cascade reactions happen in the core and the edge of the plasma, causing a direct radiation of short wave electromagnetic radiation (e.g., synchrotron, bremsstrahlung, line radiation) and high energetic particles (electrons and ions) that are absorbed in few mm of the FW surface.

The remaining part of this 'exhaust' power is released in form of electrons and ions that are trapped by the magnetic fields; they product a strong 'plasma flux' that follows the external plasma contour along the helical magnetic lines. In the divertor configuration (like in ITER and as expected for the DEMO reactors) this plasma flux is mostly directed in toroidal direction with a poloidal component that directs it to the divertor plates. This flux can be more than 100 [MW/m^2] at few centimeters from the separatrix, decreasing to 10 [MW/m^2] at about 15 [cm]. This plasma flux is responsible for the concentrated heat on the divertor plates that have to be designed to sustain heat fluxes of more than 10 [MW/m^2] [85].

The Volumetric heat generation rates set for different materials are shown in Figure 15. They were generated through a fitting equation deriving from experimental results.

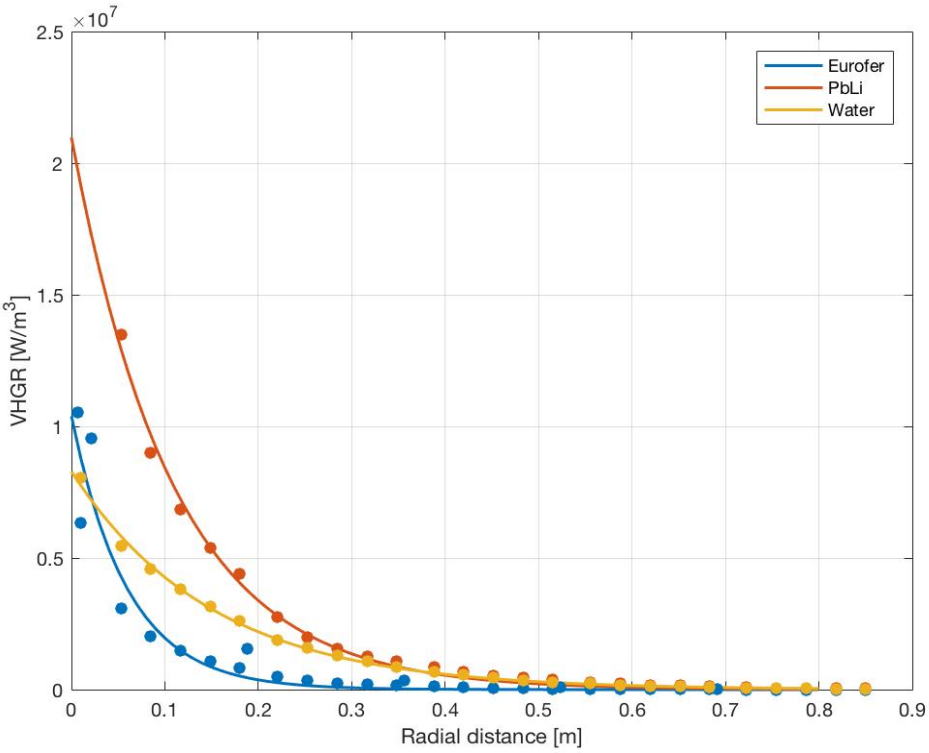

Figure 15 - Volumetric heat generation rate [86].

4 Results and discussion

A 3D simulation was performed, to carefully study the thermo-fluid-dynamic behavior of PbLi and the transport of tritium within the entire single cell of WCLL. Interface phenomena of dissociation and recombination have been considered too.

The vorticity fields in the liquid metal have been also analyzed, to better understand both the pressure variations inside it, and the stagnant areas that present maximum temperatures. The analysis presented here includes some considerations that justify the variation of tritium permeation with the radial distance from the FW and with the total tritium inventory as shown in figure 23.

4.1 Temperature and velocity

As previously explained, the first developed model concerns the study of temperature and velocity trends within the elementary cell. Considering the laminar flow in PbLi, heat transfer in PbLi, water and EUROFER has been calculated.

The temperature field in the WCLL single cell is reported in Figure 16. Two zones of maximum temperature can be identified in the PbLi; the first between first and third column of pipes, with a maximum temperature of 594 [°C], and the second near the baffle with a temperature of 541 [°C].

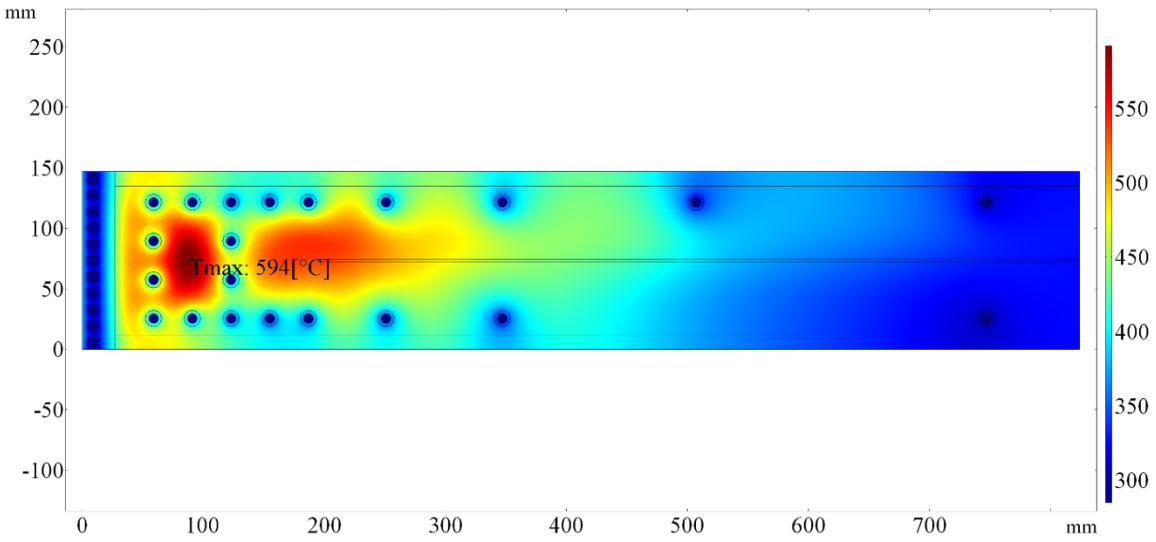

Figure 16 – Lithium-lead temperature field in a middle plane at z=L_{tor}.

The velocity field of PbLi is shown in Figure 17. The velocity presents a maximum (3.36 [mm/s]) near the fifth column of the water pipes, where the velocity field changes direction. The maximum speed is about three times higher than at the inlet. In this profile, it is also possible to observe a stagnant zone between columns 1 and 4, which contributes to the maximum temperature of 594 [°C].

The vorticity field in the PbLi is reported in Figure 18; this parameter represents the tendency of the fluid to rotate. The maximum vorticity value (1.95 [1/s]) is located near the baffle close to the pipe surface $p_{1,6}$.

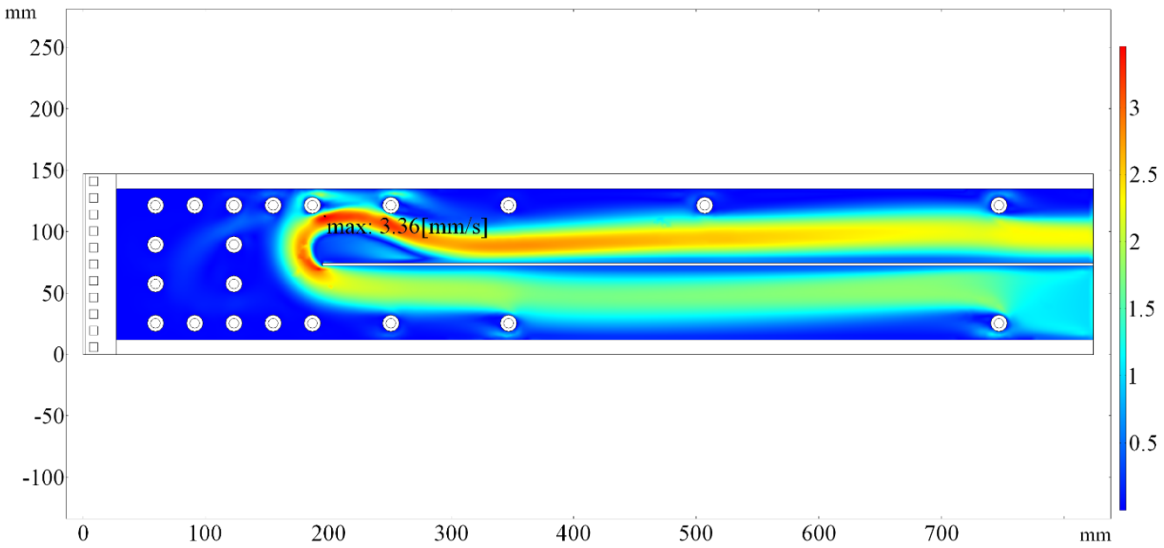

Figure 17 - Velocity field [m/s].

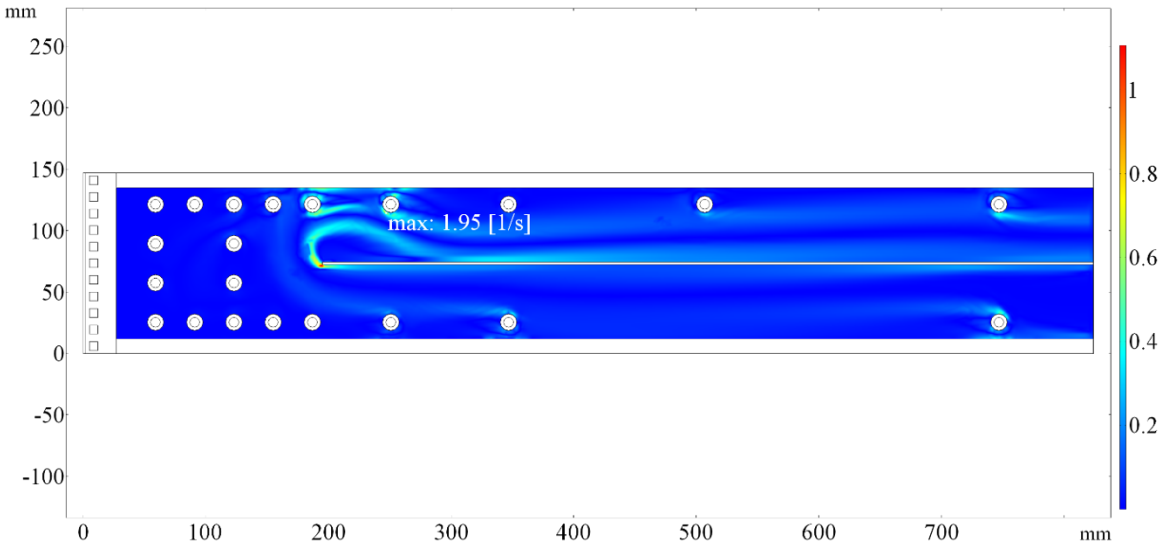

Figure 18 - Vorticity field [1/s].

4.2 Tritium transport

Tritium transport was studied in the three different materials that make up the elementary cell: EUROFER, PbLi and water. The concentration of greatest interest is the one in PbLi, and it is shown in Figure 20. The time needed to reach 90% of equilibrium is 570 [min].

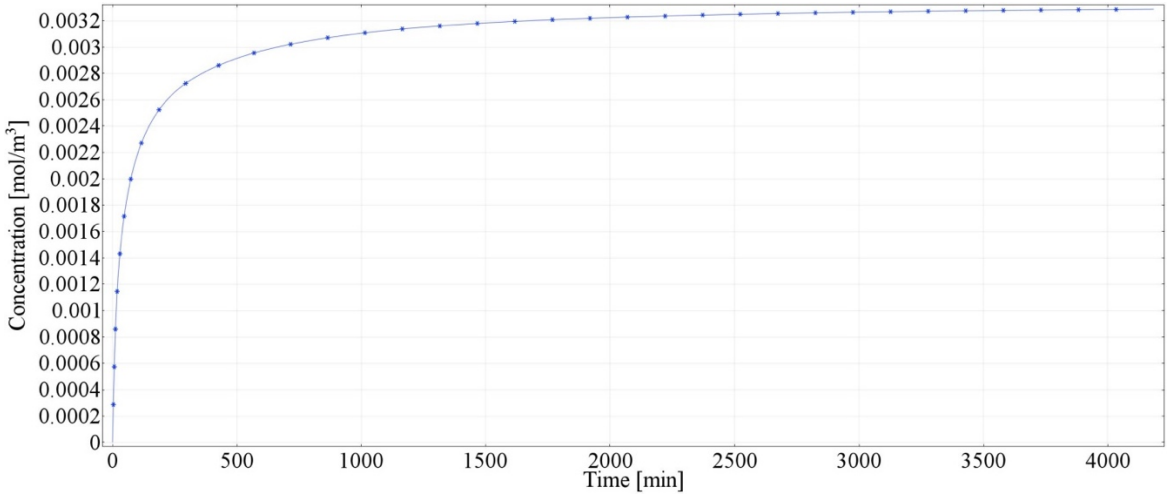

Figure 19 - Tritium concentration into PbLi.

Tritium concentration in pipes, baffle and hSPs is shown in Figure 21. The different thickness of the materials under examination causes them to reach asymptotic conditions at different times. The small thickness of 2 [mm] of the baffle allows to reach 90% of equilibrium in 90 [min]. Pipes and hSPs instead need longer times, equal to 680 and 1220 [min] respectively.

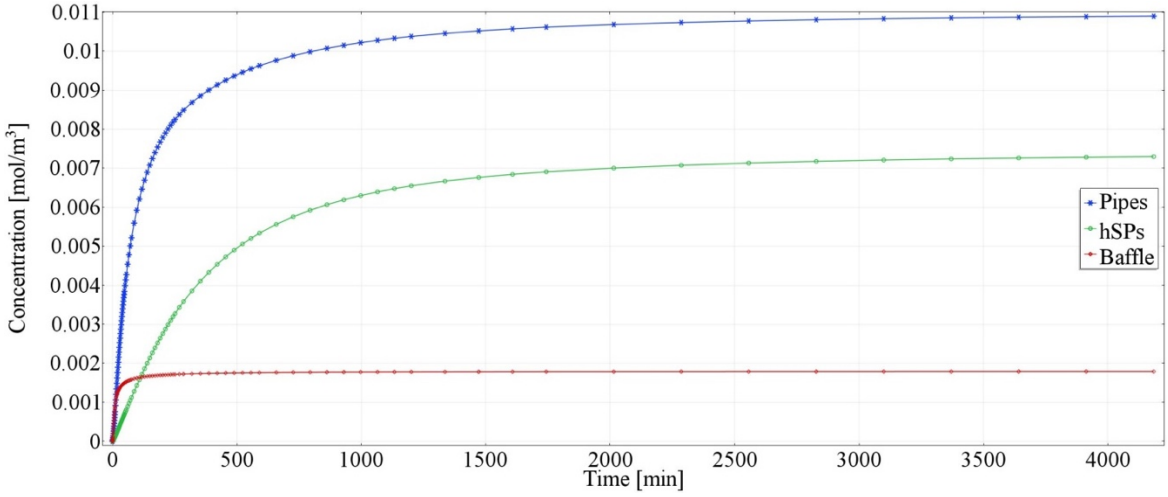

Figure 20 - Tritium concentration into pipes, hSPs and baffle.

The concentration of tritium in the water inside the BZ pipes varies while the distance from the FW increases; the results are visible in Figure 22.

In the graph, we see that the second column shows a higher asymptotic concentration than the first one; this is due to the fact that in the first column the average concentration has been calculated by considering the sum of the volumes of four pipes, whilst in the second column this sum regards only two pipes.

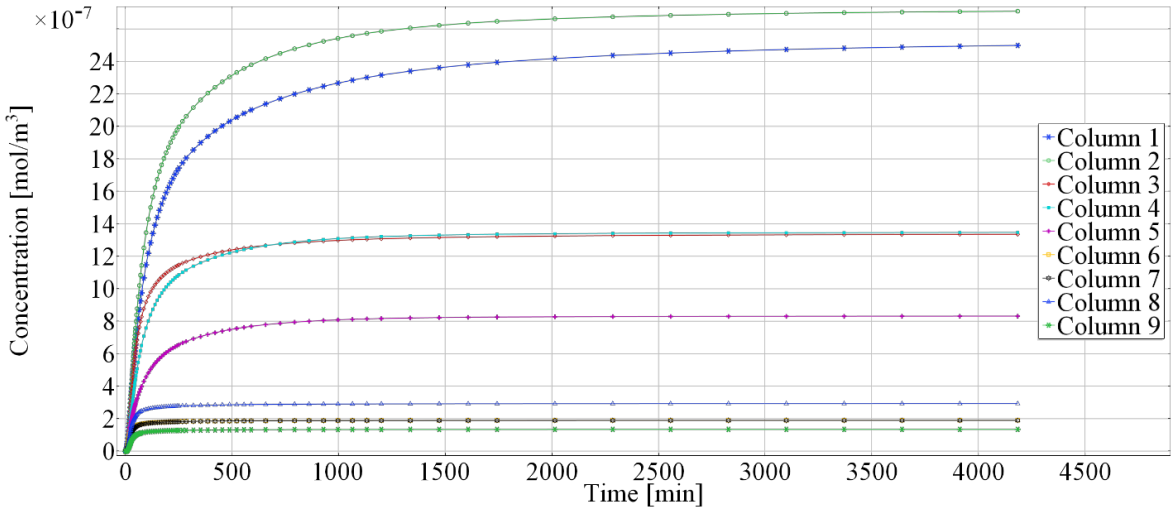

Figure 21 - Tritium concentration inside water pipes.

To better understand the influence of distance from the FW on tritium concentration, two different regions can be determined: the first one goes from the FW to the end of the baffle (region 1), whereas the second one ends at the PbLi inlet/outlet (region 2). The CFD study shows a volume of stagnant PbLi near the second column and the hSPs: the low speed of PbLi in this zone favors an increase of T concentration in the second column. The radial concentration behavior in PbLi is shown in Figure 23. This graph has been obtained by considering a cut line located in the middle plane at $Z = Z_{tor}/2$ - between the first and second row of EUROFER pipes – and the same was done between rows 3 and 4.

We see that - in region one - tritium concentration is influenced by the distance from the FW, while, in region two, there is an almost constant concentration.

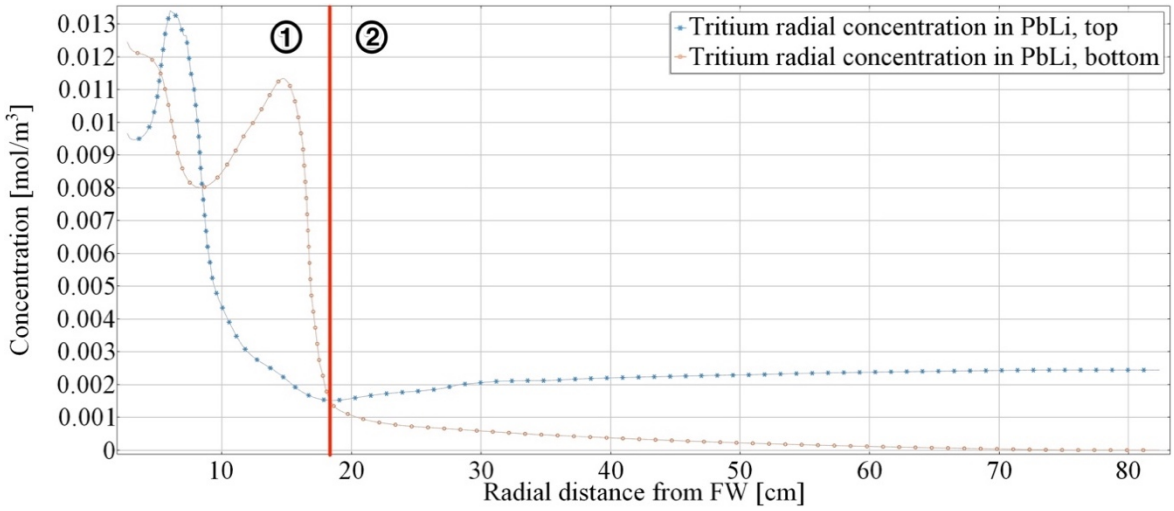

Figure 22 - Tritium radial concentration. Region 1 and 2.

Figure 24 regards the first row only: the concentration of the first four columns decreases moving away from the FW, as previously assumed. From column five to the last one, the concentration is almost constant.

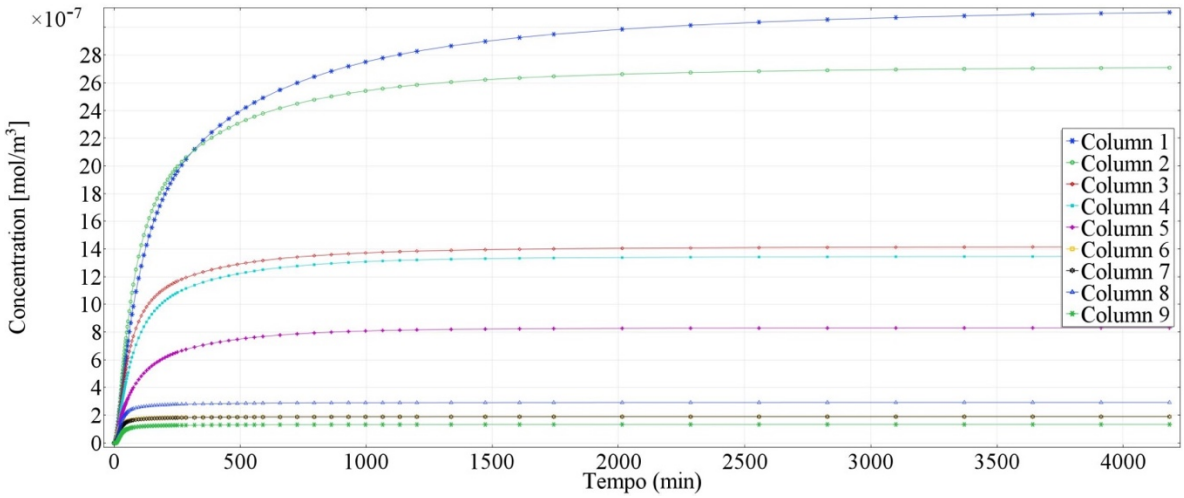

Figure 23 - Tritium concentration inside water pipes line 1.

We finally present a series of tables, which summarize the above results in terms of concentrations and times for the achievement of equilibrium (Tab. 13), inventories (Tab. 14) and losses (Tab. 15 and Fig. 25). In Table 13 only T_2 was considered because, in the study, the reactions occurring between tritium and water were neglected.

The calculation of inventories was performed by integrating the concentrations on the volume of the domain taken into consideration:

$$I_i(t) = \iiint c_i(x,t)dV_i \tag{42}$$

the subscripts represent the three reference domains for PbLi, Eurofer and Water. The percentage of tritium in the PbLi domain compared to the total inventories is 65.35% while in the Eurofer of 34.65%.

The losses are given instead by the relationship between the tritium permeated through the i-th surface and that produced in the LM domain (V_{LM}):

$$\phi(t) = \frac{\iint J_{perm}(x,t)dA_i}{\iiint s(x,t)dV_{LM}} \tag{43}$$

Table 13 - Concentration and time to reach equilibrium.

Concentration	**Equilibrium conc. [mol/m^3]**	**t* [min]**
T in Pb-15.7Li	$3.29 \cdot 10^{-3}$	570
T in EUROFER (pipes)	$1.09 \cdot 10^{-2}$	680
T in EUROFER (baffle)	$1.79 \cdot 10^{-3}$	90
T in EUROFER (hSPs)	$7.30 \cdot 10^{-3}$	1220
T_2 in Water	$1.26 \cdot 10^{-6}$	620

Table 14 - Inventories.

Inventories	**[µg]**
Pb-15.7Li	219.0
EUROFER (pipes)	14.8
Inv. in EUROFER (baffle)	1.6
Inv. in EUROFER (hSPs)	99.7
Inv. in EUROFER (total)	116.1
Inv. in Water (total)	$1.9 \cdot 10^{-3}$
Total	335.102

Table 15 - Losses.

Losses	**[%]**
hSPs	1.35
Pipes	1.41
Baffle	8.0
FW	0.14
Total	10.9

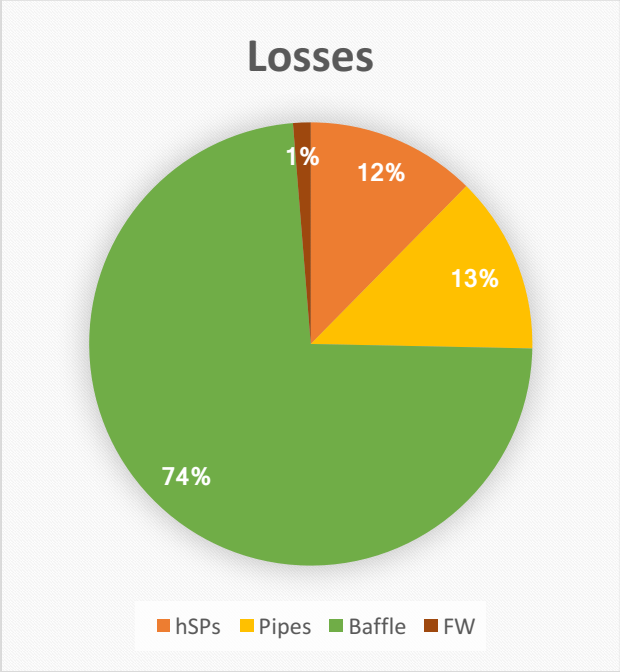

Figure 24 - Losses.

Tritium balance (Figure 26) in lithium-lead must be satisfied at each time of computational steps; for this purpose, an integral evaluation of the mass balance has been carried out by means of the following equation:

$$\oiint s(\vec{x},t)dV = \sum_{i=1}^{n_p} \oiint J_{perm,i} dA_i + \oiint J_{out}(\vec{x},t)dA + \frac{\partial}{\partial t} \oiint c_1(\vec{x},t)dV \tag{44}$$

s $[\mathrm{mol}/(\mathrm{m}^3 \cdot \mathrm{s})]$ is the tritium generation rate, V_{LM} $[\mathrm{m}^3]$ is the LM volume, n_p is the number of permeation surfaces, J_{perm} $[\mathrm{mol} \cdot/(\mathrm{m}^2 \cdot \mathrm{s})]$ is the tritium permeation flux in the A_i $[\mathrm{m}^2]$ permeation area (i.e. interface between lithium-lead and the EUROFER pipes, lithium-lead and baffle and lithium-lead and hSPs) and c_1 $[\mathrm{mol}/\mathrm{m}^3]$ is the tritium concentration in the liquid metal. This equation is an application of conservation of mass performed in the whole domain of PbLi: the amount of generated tritium must be equal to that in output plus the accumulated one.

The equation refers to the PbLi domain only, and despite this, it can approximate the total mass balance of the whole BU: in fact, the far highest concentration of tritium is inside the PbLi. Moreover, each single elementary cell confines another equal cell, and much of the permeate flow passes from cell to cell.

The average error is 2.3% and it is calculated as:

$$err_{\%} = \frac{100}{t_{fin}} \cdot \int_0^{t_{fin}} \left(\frac{\sum_{i=1}^{n_p} \oiint J_{perm,i} dA_i + \oiint J_{out}(\vec{x}, t) dA + \frac{\partial}{\partial t} \iiint c_1(\vec{x}, t) dV}{\iiint s(\vec{x}, t) dV} - 1 \right) dt \tag{45}$$

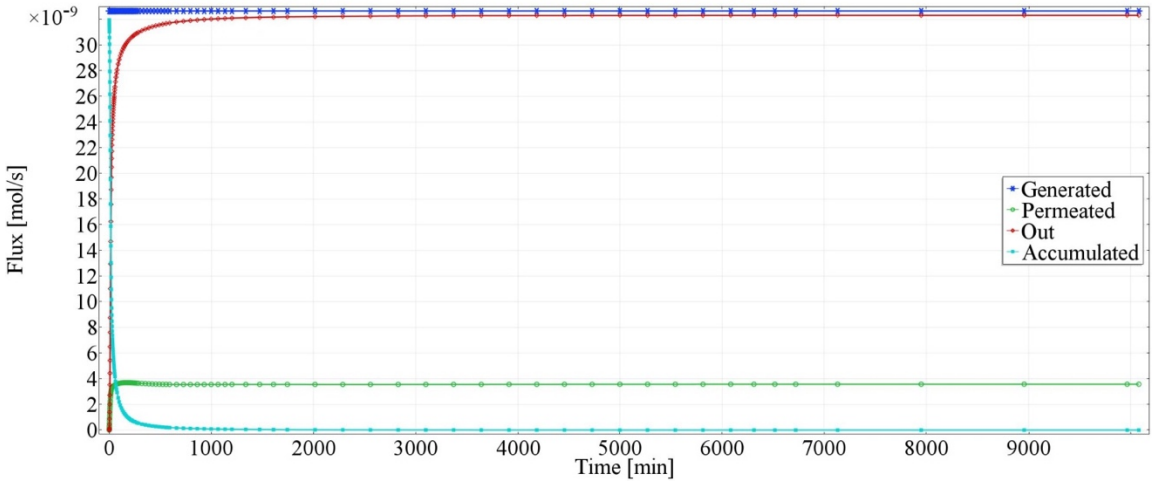

Figure 25 - Mass Balance.

5 Conclusion

The objective of this work has been a study of the tritium transport within the single WCLL cell, in order to obtain total tritium production and the amount of tritium permeated through the support structures of the elementary cells, with an accurate estimate of tritium inventory.

Starting from the thermo-fluid-dynamics analysis of PbLi and water used as a coolant, all the necessary theoretical models - necessary to estimate the amount of tritium permeated in the different interfaces - have been developed. All the phenomena relevant from a physical viewpoint have been taken into account.

It has been demonstrated that the temperature increases in the toroidal direction from the water inlet to the outlet, whereas it decreases along the radial direction; on the other hand, the average water temperature in the pipes of the breeding zone is decreasing when increasing the distance from the first wall. The temperature range in the structural material (600 [°C]), in the coolant and in the liquid breeder has values below the maximum design limits, thus guaranteeing a useful temperature margin for a future improvement of the design, optimizing the layout and the mass distribution of PbLi inside the channel. Although the maximum temperature value of PbLi (594 [°C]) is lower than the maximum tolerable limit, future studies that could include the presence of a certain level of buoyancy could further homogenize the temperature, and reduce the maximum value.

Taking into consideration the future activity of DEMO, the achievement of the asymptotic 90% tritium concentration still needs too long times, especially in PbLi and in inner pipes: the extraction and recovery of tritium could be affected by this phenomenon, that should be taken into account while estimating tritium self-sufficiency of the reactor. The complex geometry of the elementary cell plays a fundamental role in achieving the asymptotic tritium concentration, due to the stagnant areas near the FW and Baffle. The diffusion processes are therefore more relevant than those of advection. The tritium Sieverts' constant in PbLi has a great impact on the assessment of tritium losses. A weak point of PbLi is the low value of the tritium solubility constant. The slow achievement of the concentration means that, within the PbLi, non-solubilized gaseous tritium areas are created that can lead to safety problems.

Inside the elementary cell, the total tritium inventory is about 335 [μg], 65% in the PbLi, 34% in EUROFER and less than 0.1% in water. The EUROFER inventory – however small compared to the total T amount – is a relevant quantity from the radioactive safety viewpoint, since it cannot be extracted as in the case of PbLi and water.

The losses - calculated as the ratio of the permeated flow on the produced tritium - remain on values well below 10%. The biggest losses are in the Baffle domain [8%], since, in the baffle, there is the highest permeate flow ($2.63 \cdot 10^{-9}$ $[mol/s]$).

6 Reference

[1] A. Del Nevo and E. Martelli, "Final Report on Deliverable Design Description Document 2015 for WCLL (update of DDD 2014)," ENEA, 2016.

[2] "ITER," [Online]. Available: http://www.iter.org/faq#Do_we_really_know_how_much_ITER_will_cost.

[3] J. M. Arroyoa, R. Brownb, J. Harmanc, E. Rosaa and A. Ibarra, "Preliminary RAMI analysis of WCLL blanket and breeder systems," *Fusion Engineering and Design,* vol. 98–99, pp. 1719-1722, 2015.

[4] J. Freidberg, "Plasma Physics And Fusion Energy," Cambridge University Press, 2008, pp. 21-58.

[5] D. Stork, "DEMO and the Route to Fusion Power," *Intl School of Fusion Technology,* 2009.

[6] B. Christian, G. Aiello, R. Albanese, R. Ambrosino, F. Arbeiter and L. Boccacini, "Initial DEMO tokamak design configuration studies," *Fusion Engineering and Design,* Vols. 98-99, pp. 1423-1426, 2015.

[7] G. Federici, W. Biel, M. Gilbert, R. Kemp, N. Taylor and R. Wenninger, "European DEMO design strategy and consequences for materials," *Nuclear Fusion,* vol. 57, 2017.

[8] L. Boccaccini, "EU blanket design and R&D for DEMO," in *2nd EU–US DCLL Workshop*, Rice Room (6764 Boelter Hall), 14–15 November 2014.

[9] "ITER," [Online]. Available: https://www.euro-fusion.org/newsletter/self-sufficient-fusion-reactor-2/.

[10] J. Yu, "Fission-Fusion Neutron Source," *Joural of Nuclear Material,* Vols. 386-388, pp. 949- 953, 2009.

[11] J. Freidberg, in *Plasma Physics And Fusion Energy*, Cambridge University Press, 2008, pp. 21-58.

[12] L. Boccaccini, "Objectives and Status of EUROfusion DEMO Blanket Studies," *Fusion Science and Technology ,* vol. 71, 2017.

[13] L. A. Sedano, "Tritium Cycle Design for He-cooled Blankets for DEMO," Asociación EURATOM / CIEMAT para Fusión, Madrid, 2007.

[14] F. Hernández, P. Pereslavtsev, Q. Kang, P. Norajitra, B. Kiss, G. Nádasi and O. Bitz, "A new HCPB breeding blanket for the EU DEMO: Evolution, rationale and preliminary performances," *Fusion Engineering and Design,* vol. 124, pp. 882-886, 2017.

[15] P. Arena, "Thermal optimization of the Helium-Cooled Lithium Lead breeding zone layout design regarding TBR enhancement," *Fusion Engineering and Design,* vol. 124, pp. 827-831, 2017.

[16] I. Palermo, G. Veredas, J. Gómez-Ros, J. Sanz and A. Ibarra, "Neutronic design studies of a conceptual DCLL fusion reactor for a DEMO and a commercial power plant," *Nuclear Fusion,* vol. 56, 2015.

[17] P. Pereslavtseva, C. Bachmannb and U. Fischera, "Neutronic analyses of design issues affecting the tritium breeding performance in different DEMO blanket concepts," *Fusion Engineering and Design,* Vols. 109-111, pp. 1207-1211, 2016.

[18] E. Proust, L. Anzidei, G. Casini, M. Delle Donne, L. Giancarli and S. Malang, "Breeding blanket for DEMO," *Fusion Energy and Design,* vol. 22, pp. 19-33, 1993.

[19] L. Boccaccini and C. Moreno, "T transport Analyses at System level for BB / Preliminary system modelling for HCPB, WCLL, HCLL and DCLL.".

[20] I. Ricapito, "Further improvements of the water-cooled Pb–17Li blanket," *Fusion Engineering and Design,* Vols. 58-59, pp. 523-527, 2001.

[21] "AFTER ITER," [Online]. Available: https://www.iter.org/sci/iterandbeyond. [Accessed 28 07 2015].

[22] "Fusion Electricity. A roadmap to the realisation of fusion energy - EFDA," EFDA, 2012.

[23] S. Tosti and N. Gherelli, Tritium in Fusion - Production, Uses and Environmental Impact, NY: Nova Publishers, 2013.

[24] T. Tanabe, "Tritium fuel cycle in ITER and DEMO: Issues in handling large amount of fuel," *Journal of Nuclear Materials,* vol. 438, pp. S19-S26, 2013.

[25] M. Sawan and M. Abdou, "Physics and technology conditions for attaining tritium self-sufficiency for the DT fuel cycle," *Fusion Eng. Des,* vol. 81, pp. 1131-1144, 2006.

[26] A. Santucci, A. Ciampichetti, D. Demange, F. Franza and S. Tosti, "Tritium Migration in HCLL and WCLL Blankets: Impact of Tritium Solubility in Liquid Pb-17Li," in *Fusion Engineering (SOFE)*, 2013.

[27] L. Boccaccini, G. Aiello, C. Bachmann, T. Barrett, A. Del Nevo and D. Demange, "Objectives and status of EUROfusion DEMO blanket studies," *Fusion Engineering and Design,* Vols. 109-111, pp. 1199-1206, 2016.

[28] A. Del Nevo, "Integration for WCLL in 2015 / DDD 2015 for WCLL (update of DDD 2014)," ENEA, 2016.

[29] G. H. Neilson, "Magnetic Fusion Energy From Experiments to Power Plants," Elsevier, 2016.

[30] Neilson and H. George, "Magnetic Fusion Energy From Experiments to Power Plants," Elsevier, 2016.

[31] G. Belit, R. David, B. Fernández, J.-R. David, S. Javier, M. Carlos, P. Iole and I. Ángel, "Design and fabrication of a Permeator Against Vacuum prototype for small scale testing at Lead-Lithium facility," *Fusion Engineering and Design,* vol. 124, p. 871–875, 2017.

[32] M. Utili, "DCLL WORKSHOP- Tritium extraction technologies for EU DCLL," in *ENEA Experience in PbLi Technologies*, 2014.

[33] M. Utili, A. Aiello, L. Laffi, A. Malavasi and I. Ricapito, "Investigation on efficiency of gas liquid contactor used as tritium extraction unit for HCLL-TBM Pb-16Li loop," *Fusion Engineering and Design,* Vols. 109-111, pp. 1-6, 2016.

[34] M. Utili, "DCLL WORKSHOP- Tritium extraction technologies for EU DCLL," 14-15 November 2014.

[35] G. Pierini, F. Massetti and C. Rizzello, "Feasibility study of tritium recovery systems from 83Pb17Li breeding material of a D-T fusion reactor," *Fusion Technol.,* p. 463–471, 1985.

[36] F. Okino, P. Calderoni, R. Kasada and S. Konishi, "Feasibility analysis of vacuum sieve tray for tritium extraction in the HCLL test blanket system," *Fusion Eng. Des. ,* Vols. 109-111, pp. 1748-1753 , 2016.

[37] M. Mertens, D. Demange and L. Frances, "Model and simulation of a vacuum sieve tray for T extraction from liquid PbLi breeding blankets," *Fusion Engineering and Design,* vol. 112, pp. 541-547 , 2016.

[38] O. Fumito, N. Kazuyuki, Y. Yasushi and K. Satoshi, "Vacuum sieve tray for tritium extraction from liquid Pb–17Li," *Fusion Engineering and Design,* vol. 87, no. 7-8, pp. 1014-1018, 2012.

[39] H. Boniface, N. Gnanapragasam, D. Ryland, S. Suppiah and A. Perevezentsev, "Water Detritiation System for ITER—Evaluation of Design Parameters," *Fusion Science and Technology ,* vol. 71, pp. 241-245, 2017.

[40] H. A. Boniface, N. V. Gnanapragasam, D. K. Ryland, S. Suppiah and A. Perevezentsev, "Water Detritiation System for ITER—Evaluation of Design Parameters," *Fusion Science and Technology ,* vol. 71, pp. 241-245, 2017.

[41] A. Boniface, "Water Detritiation System for ITER—Evaluation of Design Parameters," *Fusion Science and Technology ,* vol. 71, pp. 241-245, 2016.

[42] M. Aldehani, "Hydrogen-Water Isotope Exchange in a Trickle Bed Column by Process Simulation and 3D Computational Fluid Dynamics Modelling," Lancaster University, 2016.

[43] Sood, Kveton, Spagnolo and Gierszewski, "DESIGN OF WATERDETRITIATION PLANT," Jan 1995.

[44] R. Causey, K. Richard and C. San Marchi, "Tritium Barriers and Tritium Diffusion in Fusion Reactors," Livermore, CA 94550.

[45] H. Rohrig, R. Hecker, J. Blumensaat and J. Schaefer, "Studies on the permeation of hydrogen and tritium in nuclear process heat installations," *Nuclear Engineering and Design,* vol. 34, pp. 157-167, 1975.

[46] C. San Marchi, B. Somerday and S. Robinson, "Permeability, solubility and diffusivity of hydrogen isotopes in stainless steels at high gas pressures. International Journal of Hydrogen Energy 32 (2007) 100 – 116.," *International Journal of Hydrogen Energy,* vol. 32, pp. 100-116, 2007.

[47] A. S. Zarchy and R. C. Axtmann, "Tritium permeation through stainless steel at ultra-low pressures.," *Journal of Nuclear Materials,* vol. 74, pp. 110-117, 1979.

[48] C. San Marchi, B. Somerday and S. Robinson, "Permeability, solubility and diffusivity of hydrogen isotopes in stainless steels at high gas pressures.," *International Journal of Hydrogen Energy,* vol. 32, pp. 100-116, 2007.

[49] H. Rohrig, R. Hecker, J. Blumensaat and J. Schaefer, "Studies on the permeation of hydrogen and tritium in nuclear process heat installations," *Nuclear Engineering and Design,* vol. 34, pp. 157-167, 1975.

[50] B. Zajec, V. Nemanic and C. Ruset, "Hydrogen diffusive transport parameters in W coating for fusion applications.," *Journal of Nuclear Materials,* vol. 412, p. 116 122, 2011.

[51] F. Franza, L. Boccaccini, A. Ciampichetti and M. Zucchetti, "Tritium transport analysis in HCPB DEMO blanket with the FUS-TPC Code," *Fusion Engineering and Design,* vol. 88, pp. 2444-2447, 2013.

[52] R. STICKNEY, "Diffusion and permeation of hydrogen isotopes in fusion reactors: A survey, The Chemistry of Fusion Technology," New York, Plenum Press, 1972, p. 241.

[53] O. Richardson, J. Nicol and T. Parnell, "The diffusion of hydrogen through hot platinum," *Philosophical magazine and journal of science,* vol. 8, no. 43, pp. 1-29, 1904.

[54] R. P.M., "Surface-limited hydrogen release and uptake in metals," *Journal of Nuclear Materials,* vol. 152, p. 246–258, 1988.

[55] R. E, W. F, W. P and W. J, "MEASUREMENTS OF SURFACE AND BULK PROPERTIES FOR THE INTERACTION OF HYDROGEN WITH INCONEL 600," *Journal of nuclear materials,* vol. 111, pp. 233-239, 1982.

[56] A. Ciampichetti, A. Aiello and G. Benamati, "An overview on tritium permeation barrier development for WCLL blanket concept," *JOURNAL OF NUCLEAR MATERIALS,* Vols. 329-333, pp. 1398-1402, 2004.

[57] G. Hollenberg, A. Terlain, E. Simonen and G. Kalinin, "Tritium/Hydrogen barrier development," in *Third international symposium of fusion nuclear tech.*, Los Angeles, 1994.

[58] G. Hollenberg, E. Simonen, G. Kalinin and A. Terlain, "TRITIUM/HYDROGEN BARRIER DEVELOPMENT," *Fusion Engineering and Design,* vol. 28, pp. 190-208, 1995.

[59] G. Takashi and J. Vargas Garcia, "Thermal barrier coatings produced by chemical vapor deposition," *Science and Technology of Advanced Materials,* vol. 4, pp. 397-402, 2003.

[60] W. Tianshi, P. Jian, B. Chi and J. Li, "Sol–gel prepared Al2O3 coatings for the application as tritium permeation barrier," *Fusion Engineering and Design,* vol. 85, pp. 1068-1072, 2010.

[61] C. L, T. R, U. M and Z. M, "Tritium transport model at the minimal functional unit level for HCLL and WCLL breeding blankets of DEMO," *Fusion Engineering and Design,* 2018.

[62] L. Candido, M. Utili, I. Nicolotti and M. Zucchetti, "Tritium transport in HCLL and WCLL DEMO blankets," *Fusion Engineering and Design,* Vols. 109-111, pp. 248-254 , 2016.

[63] F. Franza, L. Boccaccini, D. Demange and M. Zucchetti, "Tritium Permeation Issues for Helium-Cooled Breeding Blankets," in *Fusion Engineering (SOFE)*, 2013.

[64] A. Del Nevo and E. Martelli, "Design Description Document 2015 for WCLL (update of DDD 2014)," ENEA, 2016.

[65] A. Froio, F. Casella, F. Cismondi, A. Del Nevo, L. Savoldi and R. Zanino, "Dynamic thermal-hydraulic modelling of the EU DEMO WCLL breeding blanket cooling loops," *Fusion Engineering and Design,* vol. 124, pp. 887-891, 2017.

[66] A. Bejan, "Heat Transfer," Wiley, 1993.

[67] B. Rogov and I. Sokolova, "Hyperbolic Approximation of the Navier-Stokes Equations for Viscous Mixed Flows," *Fluid Dynamics,* vol. 37, no. 3, p. 377–395, 2002.

[68] R. Panton, "Incompressible Flow, 2nd ed.," John Wiley & Sons, 1996.

[69] D. Rupp and Weygand, "Loading rate dependence of the fracture toughness of polycrystalline tungsten," *J. Nucl. Mater.,* vol. 417, pp. 417-477, 2011.

[70] F. Tavassoli, "Fusion Demo Interim Structural Design Criteria (DISDC) Appendix A Material Design Limit Data A3.S18E EUROFER Steel," *Journal of Nuclear Materials,* vol. 373, pp. 1-8, 2004.

[71] A. Venturini and D. Martelli, "Literature review of PbLi alloys properties," ENEA, 2017.

[72] A. Santucci, A. Ciampichetti, D. Demange, F. Franza and S. Tosti, "Impact of tritium solubility in liquid Pb-17Li on tritium migration in HCLL and WCLL blankets," in *2013 IEEE 25th Symposium on Fusion Engineering, SOFE 2013*, San Francisco, CA, 2013.

[73] A. Santucci, A. Ciampichetti, D. Demange, F. Franza and S. Tosti, "Tritium Migration in HCLL and WCLL Blankets: Impact of Tritium Solubility in Liquid Pb-17Li," in *Fusion Engineering (SOFE)*, 2014.

[74] R. Causey, R. Karnesky and C. San Marchi, "Tritium Barriers and Tritium Diffusion in Fusion Reactors," Livermore, CA 94550.

[75] W. Farabolini and A. Ciampichetti, "Tritium Control A Major Issue for a Liquid Metal Blanket - CEA," *Fusion Engineering and Design,* vol. 81, pp. 753-761, 2006.

[76] N. Quick and H. Johnson, "Permeation and diffusion of hydrogen and deuterium in 310 stainless steel, 472K to 779K.," *Metallurgical Transactions,* Vols. 67-70, 1979.

[77] Y. Ebisuzaki, W. Kass and M. O'Keeffe, "Isotope effects in the diffusion and solubility of hydrogen in nickel.," *Journal of Chemical Physics,* vol. 46, pp. 1373-1378, 1967.

[78] C. Wilke and P. Chang, "CORRELATION OF DIFFUSION COEFFICIENTS IN DILUTE SOLUTIONS," *A.I.Ch.E. Journal,* vol. 1, no. 2, pp. 264 - 270, 1955.

[79] F. Reiter, "Solubility and diffusivity of hydrogen isotopes in liquid Pb-17Li," *Fusion Engineering and Design,* vol. 14, pp. 207-211, 1991.

[80] C. Moreno, E. Carella, D. Rapisarda, I. Fernández-Berceruelo, I. Palermo and A. Ibarra, "Tritium transport modeling at system level for the EUROfusion Dual Coolant Lithium-Lead breeding blanket," *Nuclear Fusion,* vol. 57, 2017.

[81] G. A. Esteban, A. Perujo, L. Sedano and B. Mancinelli, "The surface rate constants of deuterium in the reduced activating martensitic steel OPTIFER-IVb," *Journal of Nuclear Materials,* vol. 282, pp. 89-96, 2000.

[82] H. A.H., "Semiempirical correlation for Henry’s constants over large temperature ranges.," *AIChE Journal,* vol. 42, pp. 1491-1494, 1996.

[83] B. Bornscheina, C. Day, D. Demange and T. Pinna, "Tritium management and safety issues in ITER and DEMO breeding blankets," *Fusion Engineering and Design,* vol. 88, pp. 466-471, 2013.

[84] Aubert, "Final Report on Deliverable DDD 2016 for HCLL," 2016.

[85] Neilson and H. George, "Magnetic Fusion Energy From Experiments to Power Plants," Elsevier, 2016.

[86] A. Del Nevo and E. Martelli, "Design Description Document 2015 for WCLL (update of DDD 2014)," ENEA, 2016.